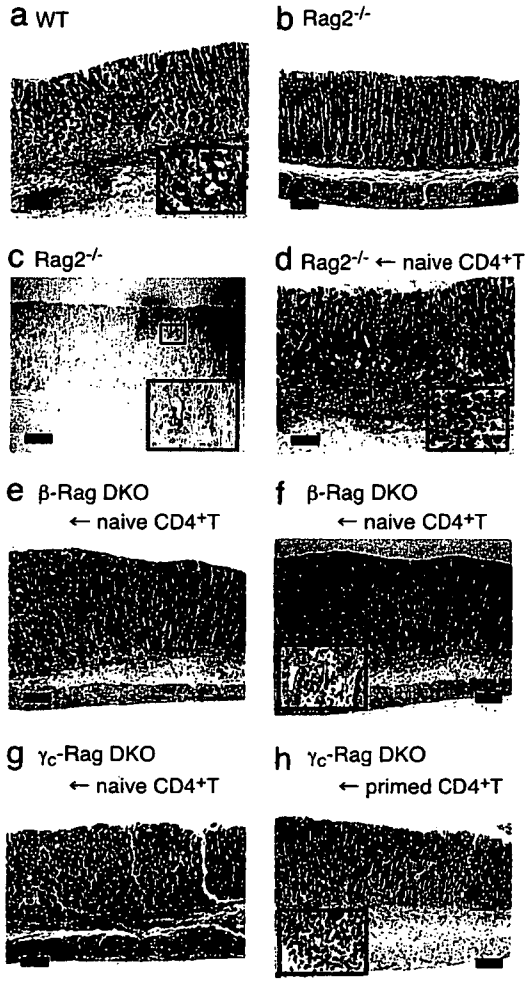

Fig. 1. Naive CD4+ T cells did not induce gastritis in *H. pylori*-infected γ_c-Rag double knockout (DKO) mice. (*a–c*) Wild-type (*a*) or Rag2$^{-/-}$ (*b* and *c*) mice were infected with *H. pylori*. Two months after the infection, gastric specimens were prepared. (*d–h*) Rag2$^{-/-}$ (*d*), β-Rag DKO (*e* and *f*), and γ_c-Rag DKO (*g* and *h*) mice were infected with *H. pylori*. Two months after the infection, naive (*d–g*) or primed (*h*) splenic CD4+ T cells were transferred. Two months after the cell transfer, gastric specimens were prepared. Specimens were stained with H&E (*a*, *b*, *d*, *e*, *g*, and *h*), anti-*H. pylori* antisera (brown) (*c*), or chloroacetate esterase (red) for infiltrated neutrophils and mast cells (*f*). (Scale bars: 200 μm.)

***H. pylori* Antigen-Specific CD4+ T Cells Are Indispensable for Induction of Gastritis.** Primary gECs secrete MIP-2, a functional homolog of IL-8, on *H. pylori* infection *in vitro*, and the amount produced by Rag2$^{-/-}$ gECs was comparable to that produced by wild-type gECs [supporting information (SI) Fig. 5*a*]. CD4+ T cells isolated from the gLP of *H. pylori*-infected mice were able to produce larger amounts of MIP-2 than splenic CD4+ T cells from the same mice in response to *H. pylori* antigens (SI Fig. 5*b*). Moreover, the amounts of MIP-2 produced by gLP CD4+ T cells were much larger than those produced by gECs (compare SI Fig. 5 *a* and *b*). The importance of CD4+ T cells for neutrophil infiltration on *H. pylori* infection was further confirmed by the depletion of CD4+ T cells from wild-type mice that had already developed gastritis by *H. pylori* infection. After depleting CD4+ T cells by the i.v. injection of anti-CD4 mAb, the gastritis became milder (Table 1 and SI Fig. 6 *a* and *b*), and the number of bacteria in the gastric mucosa increased (Table 1). These results indicate the critical role of CD4+ T cells for both triggering and maintaining gastritis. When CD4+ T cells from OT-II transgenic mice on a Rag2$^{-/-}$ background (OT-II-Rag mice), specific for an ovalbumin ($OVA_{323-339}$ peptide on an MHC class II molecule I-A^b), were transferred into *H. pylori*-infected Rag2$^{-/-}$ mice, no gastritis was induced (SI Fig. 6*c*). Similarly, when OT-II-Rag mice were infected with *H. pylori*, no gastritis was induced despite the presence of CD4+ T cells (Table 1 and SI Fig. 6*d*). Furthermore, when OVA protein or $OVA_{323-339}$ peptide was administered into *H. pylori*-infected OT-II-Rag mice, no inflammation was observed, although CD4+ T cells were activated in these mice (Table 1, SI Fig. 6*e*, and data not shown). These results collectively indicate the importance of *H. pylori* antigen recognition by CD4+ T cells in the induction of gastritis.

CD4+ T Cells Are Not Primed with *H. pylori* Antigen in γ_c-Rag DKO Mice. IFNγ, a key cytokine for Th1 immune responses, is important for the pathogenesis of *H. pylori*-induced gastritis (14). Natural killer (NK) cells and antigen-presenting cells (APCs) including DCs are able to produce IFNγ to prevent bacterial infection (15). The interaction between DCs and NK cells enhances the production of IFNγ during *H. pylori* infection (16, 17). To test the importance of DC–NK interaction in the *H. pylori*-induced inflammatory response, we transferred splenic CD4+ T cells into *H. pylori*-infected IL-2 receptor β chain (IL-2Rβ)$^{-/-}$Rag2$^{-/-}$ (β-Rag DKO) mice and cytokine receptor common γ chain (γ_c)$^{-/-}$Rag2$^{-/-}$ DKO (γ_c-Rag DKO) mice. These mice lack NK cells because of impaired IL-15 signaling, which is critical for NK cell development (18, 19). In addition, the production of IL-12 and IFNγ by APCs from these mice is impaired (20). As shown in Fig. 1 *e* and *f*, gastritis was induced in *H. pylori*-infected β-Rag DKO mice when naive CD4+ T cells were transferred. Clearance of bacteria was also achieved by the naive CD4+ T cell transfer (Table 1), indicating that NK cells and NK–DC interaction are dispensable for the induction of gastritis by *H. pylori* infection.

Surprisingly, there was no gastritis induced in γ_c-Rag DKO mice even after the transfer of naive CD4+ T cells (Fig. 1*g*), NK cells (SI Fig. 7*a*), or NK cells with naive CD4+T cells (SI Fig. 7*b*), suggesting that γ_c-Rag DKO mice have additional defects compared with β-Rag DKO mice. Interestingly, when splenic CD4+ T cells isolated from *H. pylori*-infected wild-type mice were transferred, gastritis was induced in *H. pylori*-infected γ_c-Rag DKO mice (Fig. 1*h*), and the clearance of bacteria was evident (Table 1). These results suggest that CD4+ T cells were not primed in γ_c-Rag DKO mice. In fact, splenocytes from these mice did not respond to DCs preincubated with *H. pylori* lysate, whereas splenocytes from wild-type mice infected with *H. pylori* strongly responded and produced IFNγ in response to the same DC preparation (data not shown). It should be noted that there were no apparent defects in DCs from γ_c-Rag DKO mice compared with those from wild-type mice with regard to their ability to induce T cell activation and present antigen as examined by the induction of CD69 expression and IFNγ production by splenic CD4+ T cells (SI Fig. 8).

PPs Are a Critical Tissue for Priming CD4+T Cells with *H. pylori* Antigen. One difference between β-Rag DKO and γ_c-Rag DKO mice is that the latter lack gut-associated lymphoid tissues (GALT) such as PPs and isolated lymphoid follicles (ILFs) due to impaired IL-7 signaling (21) (Fig. 2 *a–d*). Thus, we hypothesized that CD4+ T cells are primed in GALT such as PPs or ILFs. To test this possibility, we generated PP-null mice by administration of anti-IL-7Rα mAb *in utero* (22) (Fig. 2 *e* and *f*). As observed in γ_c-Rag DKO mice, no gastritis was induced in PP-null mice 2 months after *H. pylori* infection, and a large number of *H. pylori* was detected in the gastric mucosa (Fig. 2 *h* and *i* and Table 1). We also generated PP-null mice on a Rag2$^{-/-}$ background (PP-null-Rag2$^{-/-}$ mice) (Fig. 2*g*). The adoptive transfer of CD4+ T cells from *H. pylori*-infected wild-type mice, but not naive CD4+ T cells, induced strong inflammation in PP-null-Rag2$^{-/-}$

Table 1. PP-dependent bacterial clearance in *H. pylori* infection

Mouse*	*n*	Cells transferred†	Bacterial colonization,‡ cfu/g tissue × 10^{-6}	Neutrophils, average (range)	Active inflammation, average (range)	GAIS,§ average (range)
Wild type	7	None	2.2 ± 1.3	1.6 (0–3)	1.4 (0–3)	13.6 (0–34)
Wild type	4	$CD4^+$ T cell-depleted	25 ± 7	0 (0)	1.0 (0–2)	0 (0)
$Rag2^{-/-}$	4	None	14 ± 4	0 (0)	0 (0)	0 (0)
$Rag2^{-/-}$	5	Naive $CD4^+$ T	0.15 ± 0.17	2.0 (2)	2.0 (2)	5.0 (2–8)
$Rag2^{-/-}$	5	OT-II-Rag $CD4^+$ T	34 ± 11	0 (0)	0 (0)	0 (0)
β-Rag DKO	4	Naive $CD4^+$ T	0.67 ± 0.39	1.5 (1–2)	1.3 (1–2)	9.2 (3–18)
γ_c-Rag DKO	6	Naive $CD4^+$ T	18 ± 11	0 (0)	0 (0)	0 (0)
γ_c-Rag DKO	6	Primed $CD4^+$ T	0.22 ± 0.39	0.66 (0–1)	1.5 (0–2)	1.6 (0–5)
γ_c-Rag DKO	3	Primed $CD4^+$ T from PPs	<0.01	1.0 (1)	2.0 (2)	1.0 (0–2)
γ_c-Rag DKO	3	Primed $CD4^+$ T from mLN	0.88 ± 0.78	0.5 (0–1)	1.5 (1–2)	4.0 (3–5)
γ_c-Rag DKO	3	Primed $CD4^+$ T by coccoid form	1.8 ± 1.6	0.33 (0–1)	0.66 (0–1)	2.0 (0–6)
PP-null-wild type	8	None	16 ± 9	0 (0)	0.37 (0–1)	0 (0)
PP-null-$Rag2^{-/-}$	3	Naive $CD4^+$ T	5.3 ± 4.0	1.0 (0–2)	1.0 (0–2)	4 (0–7)
PP-null-$Rag2^{-/-}$	3	Primed $CD4^+$ T	0.53 ± 0.28	2.6 (2–3)	2.6 (2–3)	21 (13–33)

*All mice were on a C57BL/6 background. Although not shown, the degrees of bacterial colonization in β-Rag DKO, γ_c-Rag DKO, and PP-null-$Rag2^{-/-}$ mice without $CD4^+$ T cell transfer were similar to those of $Rag2^{-/-}$ mice.

†Splenocytes were used for cell transfer unless otherwise stated. Five million cells were transferred except for the transfer of PP-derived cells, where 5×10^5 cells were used.

‡Mean ± SD.

§Gland active inflammatory score. See *Materials and Methods*.

mice just as in the γ_c-Rag DKO mice (Fig. 2 *j* and *k* and Table 1). These results strongly suggest that PPs are critical for priming $CD4^+$ T cells in *H. pylori* infection, but dispensable for the effector phase.

The Coccoid, but Not Helical, Form of *H. pylori* Is Phagocytosed by DCs in PP. Although *H. pylori* is helical in the stomach, it transforms to the coccoid form under anaerobic conditions, such as in the small intestine (23). Interestingly, the coccoid form of *H. pylori* induced higher IL-12 production from bone marrow-derived cells (BMDCs) than the helical form (SI Fig. 9). There is a possibility that *H. pylori* transforms to the coccoid form in the intestine and is then captured by DCs present in PPs to induce a Th1 response. To test this possibility, the coccoid and helical forms of *H. pylori* were inoculated into ligated small intestinal loops. As shown in Fig. 3*a*, immunofluorescence staining detected *H. pylori* in the subepithelial dome (SED) region of PPs in a time-dependent manner, and the number of bacteria in the SED region inoculated with the coccoid form was larger than that inoculated with the helical form of *H. pylori*. In addition, double immunofluorescence staining with anti-*H. pylori* antibody and anti-CD11c mAb demonstrated that the bacteria were captured by $CD11c^+$ DCs in the SED region (Fig. 3*b*). Although the helical form of *H. pylori* kept the rod shape 1.5 h after inoculation (SI Fig. 10 *a* and *b*), the bacteria phagocytosed by $CD11c^+$ DCs in PPs were round (SI Fig. 10 *c* and *d*). These results suggest that the coccoid, but not the helical, form of *H. pylori* is captured by DCs in PPs and activates immune responses by generating *H. pylori*-specific pathogenic $CD4^+$ T cells. Consistent with this observation, $CD4^+$ T cells from the PPs as well as mesenteric lymph node (mLN) of *H. pylori*-infected wild-type mice were also able to eliminate the bacteria in γ_c-Rag DKO mice infected with *H. pylori* (Table 1).

When wild-type mice were infected with the coccoid form of *H. pylori*, gastritis was not induced because the coccoid form of *H. pylori* was unable to colonize in the stomach (Fig. 4*a* and data not shown). However, $CD4^+$ T cells from these mice induced gastritis in γ_c-Rag DKO mice infected with the helical form of *H. pylori* (Fig. 4 *b* and *c* and Table 1). These results indicate that $CD4^+$ T cells primed with the coccoid form of *H. pylori* in the intestine are sufficient to induce inflammation in the stomach infected with the helical form of *H. pylori*.

Discussion

We showed here that *H. pylori* antigen-specific $CD4^+$ T cells are required to induce and maintain gastritis on infection with *H. pylori*. Because *H. pylori* interacts with and injects pathological molecules into gECs, it is generally thought that neutrophils infiltrating the gLP are attracted by chemokines produced by gECs. However, neutrophil infiltration was not observed in $Rag2^{-/-}$ mice, although gECs of $Rag2^{-/-}$ mice were able to secret MIP-2 on *H. pylori* infection. Thus, the secretion of chemokines by gECs seems insufficient for the induction of gastritis. In addition, adoptive transfer of $CD4^+$ T cells recognizing *H. pylori*-independent antigens did not induce gastritis, suggesting that *H. pylori*-specific $CD4^+$ T cells directly or indirectly regulate production of chemokines that attract neutrophils. In fact, a large amount of MIP-2 was produced by activated $CD4^+$ T cells derived from the gLP of *H. pylori*-infected mice. In addition, infiltrated neutrophils were located around $CD4^+$ T cells in the gLP of *H. pylori*-infected mice (data not shown). It is known that another keratinocyte-derived chemokine is able to recruit neutrophils. However, the amounts of keratinocyte-derived chemokine produced by both gECs and CD4 T cells were much lower than those of MIP-2 (data not shown).

Oral or intra-PP immunization with *H. pylori* antigens was effective in enhancing *H. pylori*-specific $CD4^+$ T cell responses and reducing *H. pylori* colonization in the stomach (24, 25). These reports are consistent with our current observation that PPs play critical roles in priming $CD4^+$ T cells, and *H. pylori* is indeed captured by DCs in PPs. *H. pylori* antigen-specific $CD4^+$ T cells would be primed by DCs in PPs or mLNs where DCs migrate after capturing antigens. Interestingly, $CD4^+$ T cells cannot be primed by DCs in the gLP or gEC, both of which are capable of expressing class II MHC and presenting antigens. The lack of antigen presentation is partly due to the fact that the helical form of *H. pylori* is resistant to phagocytosis in a type IV secretion system-dependent manner, although the molecular mechanisms of antiphagocytic activity remain to be determined (26). It should be noted that the transformation of the helical to the coccoid form is accompanied by changes in the composition

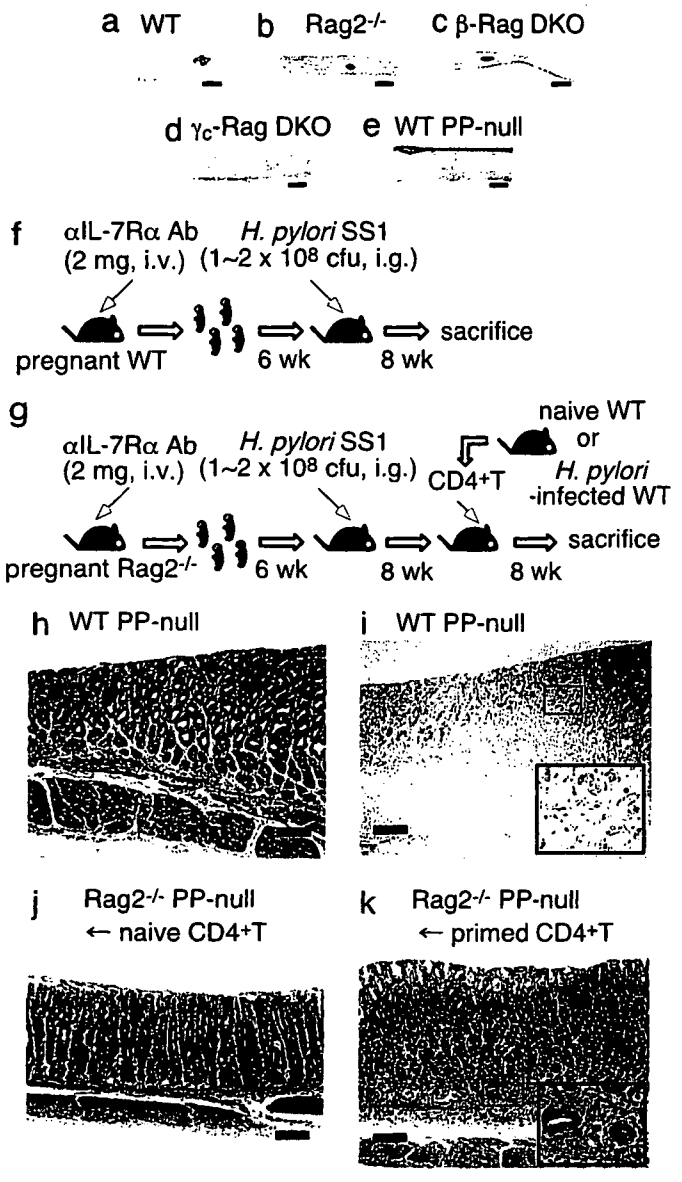

Fig. 2. PPs are critical for the priming of CD4+ T cells in *H. pylori* infection. (*a–e*) Small intestines from wild-type (WT) (*a*) and PP-null (*e*) mice were stained with anti-B220 mAb, and small intestines from Rag2$^{-/-}$ (*b*), β-Rag DKO (*c*), and γ_c-Rag DKO (*d*) mice were stained with anti-CD45 mAb. (*f* and *g*) Schemes of the generation of PP-null WT (*f*) or PP-null-Rag2$^{-/-}$ (*g*) mice. (*h* and *i*) PP-null WT mice were infected with *H. pylori*. Two months after the infection, gastric specimens were prepared. (*j* and *k*) PP-null-Rag2$^{-/-}$ mice were infected with *H. pylori*. Two months after the infection, naive (*j*) or primed (*k*) splenic CD4+ T cells were transferred. Two months after the cell transfer, gastric specimens were prepared. Specimens were stained with H&E (*h*, *j*, and *k*) or anti-*H. pylori* antisera (brown) (*i*). (Scale bars: 200 μm.)

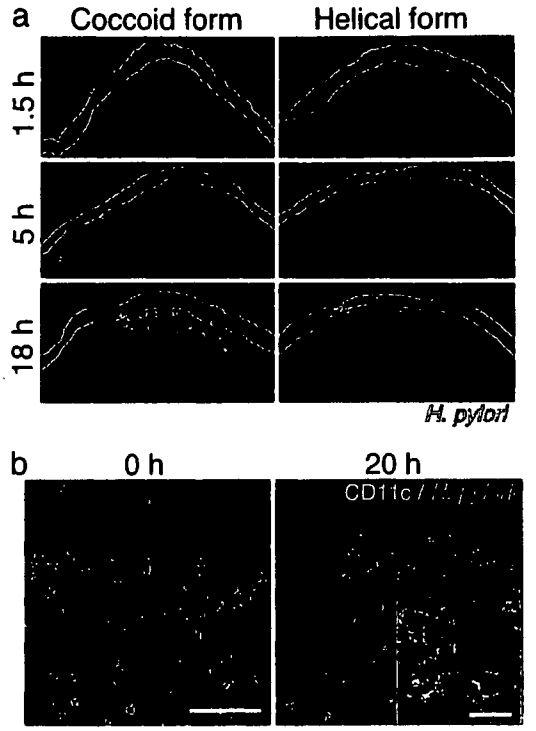

Fig. 3. The coccoid form of *H. pylori* is captured by DCs in PPs. The coccoid or helical form of *H. pylori* was inoculated into the ligated small intestines of wild-type mice. (*a*) After the indicated incubation times, PPs were stained with anti-*H. pylori* antibody. (*b*) Twenty hours after inoculation of the coccoid form, PPs were stained with anti-CD11c mAb (green) and anti-*H. pylori* antibody (red). (Scale bars: 0 h,100 μm; 20 h, 20 μm.)

of surface proteins and/or carbohydrates, which may make the bacteria susceptible to phagocytosis (27, 28), a subject worthy of further studies. It has been shown that mast cells are able to present *H. pylori* antigens to *H. pylori*-specific CD4+ T cells, which in turn activate mast cells to degranulate (29). When we infected W/W^v and Sl/Sl^d mice lacking mast cells with *H. pylori*, gastritis was readily induced in both strains of mice on infection (S.N., T.Y., Y.B., and S.K., unpublished data), indicating that mast cells are not essential in priming CD4+ T cells. In an *in vitro* experiment, BMDCs infected with the coccoid form of *H. pylori* produced larger amounts of IL-12 than those infected with the helical form of *H. pylori*, suggesting that the coccoid form of *H. pylori* easily induces Th1 immune responses on *H. pylori* infection.

Importantly, CD4+ T cells primed with the coccoid form of *H. pylori* were able to induce gastritis in *H. pylori*-infected GALT-null γ_c-Rag DKO mice where CD4+ T cells are not

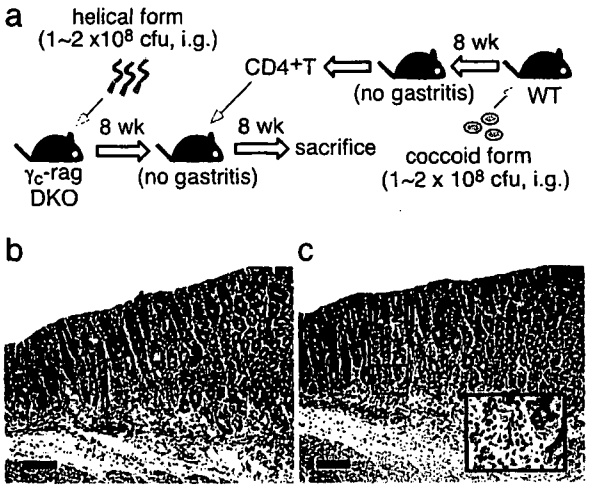

Fig. 4. Gastritis is induced by CD4+ T cells primed by the coccoid form of *H. pylori*. Two months after infection of γ_c-Rag DKO mice with the helical form of *H. pylori*, splenic CD4+ T cells from wild-type (WT) mice orally infected by the coccoid form of *H. pylori* were transferred to the infected γ_c-Rag DKO mice (*a*). Two months after the cell transfer, gastric specimens were prepared. Specimens were stained with H&E (*b*) or chloroacetate esterase (red) for infiltrated neutrophils and mast cells (*c*). (Scale bars: 200 μm.)

primed with *H. pylori* antigen at all. Thus, the following scenario emerges from our results: *H. pylori* transforms to the coccoid form when entering the intestinal tract and is captured by DCs in PPs. *H. pylori* antigens presented by DCs are recognized by $CD4^+$ T cells in PPs or mLN, and activated T cells migrate to the gastric mucosa to induce and maintain inflammatory responses. We noted that PP-null-$Rag2^{-/-}$ mice exhibited modest inflammation in the stomach after naive $CD4^+$ T cell transfer, compared with γ_c-Rag DKO mice, which showed no sign of inflammation. Because treatment by anti-IL-7Rα mAb *in utero* suppresses PP development, but leaves ILFs and recently discovered villous M cells (30) intact, ILFs and/or villous M cells may also participate in the capture of *H. pylori* in the intestine. Although luminal antigens can be taken up by M cells located over the follicular epithelia of ILF, the tissue is predominantly occupied by B cells (31). Furthermore, in a separate study, we have shown that no apparent organized lymphoid structure is developed under villous M cells (data not shown).

H. pylori is also implicated in the cause of other diseases such as idiopathic thrombocytopenic purpura (32) and Sjögren syndrome (33). Indeed, it has been shown that T cells migrate from the intestine to the salivary gland in Sjögren syndrome patients (34). It will be of interest to examine the functional relationship between these diseases and the coccoid form of *H. pylori* captured via PPs.

Materials and Methods

Mice. All mice used in this study were on a C57BL/6 background and were maintained at Taconic (Germantown, NY) or in our animal facility under specific pathogen-free conditions. Wild-type C57BL/6 mice were purchased from Sankyo Labo Service (Shizuoka, Japan) and CLEA Japan (Tokyo, Japan). $Rag2^{-/-}$ mice, γ_c-Rag DKO mice, and OT-II-Rag mice were obtained from Taconic. IL-$2R\beta^{-/-}$ mice (35) were generously provided by T. W. Mak (Ontario Cancer Institute, Toronto, ON, Canada). β-Rag DKO mice were obtained by crossing IL-$2R\beta^{-/-}$ with $Rag2^{-/-}$ mice (20). All experiments were approved by the Animal Care and Use Committee of the Keio University School of Medicine and were performed in accordance with institutional guidelines.

Antibodies. Fluorescein-conjugated antibodies for flow-cytometric analysis and biotin anti-mouse $CD2_c$ (HL3) were purchased from BD Bioscience (San Jose, NJ). Anti-*H. pylori* antibodies were purchased from Biomeda (Foster City, CA) or DAKO (Glostrup, Denmark).

Bacteria. *H. pylori* strain SS1, a mouse-adapted human isolate, was used for all experiments. To prepare the helical form of *H. pylori*, SS1 was grown on 5% sheep blood agar plates for 2 days. Before inoculating into mice, bacteria were grown in *Brucella* broth with 5% FCS overnight at 37°C under microaerobic conditions with gentle agitation. To prepare the coccoid form, SS1 was grown on 5% sheep blood agar plates under microaerobic conditions for 3 days at 37°C and then cultured under anaerobic conditions for 7 days at 37°C.

***In Vivo* Infection of Mice.** Bacteria were prepared from logarithmic phase cultures. Mice were intragastrically infected with $1–2 \times 10^8$ cfu *H. pylori* in 0.15 ml of broth. After the indicated time period, mice were killed and the stomach was aseptically removed. The stomach was then bisected along the greater and lesser curvatures. Half of the stomach was homogenized for the determination of bacterial colonization by a plate-dilution method. The rest of the stomach was sectioned transversely into two strips for frozen and paraffin-embedded sections.

***In Situ* Infection of Intestinal Loop.** Wild-type mice (6-week-old females) were anesthetized by an i.m. injection of 2 mg of ketamine hydrochloride (Sankyo, Tokyo, Japan) and 0.1 mg of Xylazine per mouse. An ≈4-cm-long piece of the small intestine containing one or two PPs was ligated at both ends with surgical thread. *H. pylori* (1×10^9) suspended in 0.2 ml of saline was inoculated into the loop. After the indicated time periods, PPs were removed and extensively washed with PBS. After fixation in 4% paraformaldehyde in PBS, specimens were processed for histopathological examination.

Generation of PP-Null Mice. PPs were depleted from a small intestine as previously described (22). Briefly, 14.5 days postcoitum pregnant wild-type or $Rag2^{-/-}$ mice were i.v. injected with 2 mg of anti-IL-7Rα mAb (A7R34; kindly provided by S.-I. Nishikawa, RIKEN CDB, Kobe, Japan). To confirm the depletion of PPs, a dissected small intestine from one of the offspring was fixed with acetone and stained with anti-B220 or anti-pan CD45 mAb (BD Biosciences).

Adoptive Transfer of $CD4^+$ T Lymphocytes. Naive or *H. pylori* antigen-primed $CD4^+$ T cells were purified from splenocytes, mLN, and PPs by using anti-mouse CD4-microbeads and AutoMACS (Miltenyi Biotech, Sunnyvale, CA) according to the manufacturer's instruction. The purity of isolated cells was >95%. Isolated cells (5×10^6 per mouse for splenocytes and mLN, 5×10^5 per mouse for PP-derived cells) were injected i.v. into recipient mice infected with *H. pylori* for 8 weeks. Eight weeks after the transfer, mice were killed for the indicated analyses.

Histological Analysis. An excised stomach was fixed in a neutral-buffered 10% formalin solution and cut into four strips. Samples were processed by standard methods, embedded in paraffin, and sectioned at 4 to 5 μm. Specimens were stained with H&E or used for cytochemical and immunohistochemical studies. The Leder method was used to assess naphtol-AS-D-chloroacetate esterase detection (36). Immunohistochemical analysis was performed with formalin-fixed and paraffin-embedded tissue sections by using heat-induced epitope retrieval and the ABC (Vectastain ABC kit; Vector Laboratories, Burlingame, CA) method. Anti-*H. pylori* serum from DAKO was used for *H. pylori* staining. In some cases, frozen sections (7 μm) were prepared, fixed with 4% paraformaldehyde in PBS, and blocked with 2% BSA-PBS, and immunofluorescence was performed using the tyramide amplication method (TSA-Plus Fluorescein System; PerkinElmer Life and Analytical Sciences, Boston, MA) and then incubated with anti-*H. pylori* antibody from Biomeda, followed by Cy5 (GE Healthcare Bioscience AB, Uppsala, Sweden) or TRITC-linked rabbit IgG (Sigma–Aldrich, St. Louis, MO). The specimens were mounted with Vectashield (Vector Laboratories) and examined with a confocal laser-scanning microscope LSM510 by using version 3.2 software (Carl Zeiss, Thornwood, NY). The zymogenic zone of middle corpus ≈3 mm from the FS/Z transition zone was examined in each sample.

Histological Score. For assessment of gastric histopathology, blinded sections stained with H&E were examined by light microscopy. Neutrophil infiltration was assessed by the presence of neutrophils in the gastric mucosa. Active inflammation was assessed by the degree and area of damages of mucosal tissue and muscular layers because of infiltrations of neutrophils, lymphocytes, and/or macrophages. The scoring was graded as 0 (no), 1 (mild), 2 (moderate), or 3 (severe). The total number of glands with neutrophil infiltration in the crypt and lumen was also counted to produce a gland active inflammatory score.

Whole-Mount Immunohistochemistry. Small intestines were removed and stained with antibodies as described previously (37). Briefly, small intestines were washed, incubated twice in HBSS containing 5 mM EDTA at 37°C for 20 min, and fixed with ice-cold formalin

for 1 h. After blocking, specimens were incubated with biotin-conjugated anti-B220 mAb for wild-type mice or anti-CD45 mAb for mice on a Rag2$^{-/-}$ background in Solution A containing 0.6% Triton X-100 and 0.1% BSA for 1 h, incubated with ABC reagent (Vector Laboratories) at room temperature for 2 h, and reacted with diaminobenzidene.

We thank Drs. S.-I. Nishikawa and T. W. Mak for valuable materials; Dr. L. K. Clayton for valuable discussion and critical reading of the manuscript; and M. Motouchi and N. Yumoto for animal care. This work was supported by the Waksman Foundation of Japan (S.N.), the Uehara Memorial Foundation, the Tokyo Biochemical Research Foundation, Japan Society for the Promotion of Science Grant-in-Aid 18659141, Scientific Research on Priority Areas Grant-in-Aid 14021110, a National Grant-in-Aid for the Establishment of a High-Tech Research Center in a Private University, a grant for the Promotion of the Advancement of Education and Research in Graduate Schools, and a Scientific Frontier Research Grant from the Ministry of Education, Culture, Sports, Science, and Technology, Japan.

1. Covacci A, Telford JL, Del Giudice G, Parsonnet J, Rappuoli R (1999) *Science* 284:1328–1333.
2. Ernst PB, Gold BD (2000) *Annu Rev Microbiol* 54:615–640.
3. Uemura N, Okamoto S, Yamamoto S, Matsumura N, Yamaguchi S, Yamakido M, Taniyama K, Sasaki N, Schlemper RJ (2001) *N Engl J Med* 345:784–789.
4. Baldari CT, Lanzavecchia A, Telford JL (2005) *Trends Immunol* 26:199–207.
5. Cover TL, Blanke SR (2005) *Nat Rev Microbiol* 3:320–332.
6. Eaton KA, Ringler SR, Danon SJ (1999) *Infect Immun* 67:4594–4602.
7. Pappo J, Torrey D, Castriotta L, Savinainen A, Kabok Z, Ibraghimov A (1999) *Infect Immun* 67:337–341.
8. Panthel K, Faller G, Haas R (2003) *Infect Immun* 71:794–800.
9. Lundgren A, Trollmo C, Edebo A, Svennerholm AM, Lundin BS (2005) *Infect Immun* 73:5612–5619.
10. Yamaguchi H, Osaki T, Takahashi M, Taguchi H, Kamiya S (1999) *FEMS Microbiol Lett* 175:107–111.
11. Reynolds DJ, Penn CW (1994) *Microbiology* 140:2649–2656.
12. Narikawa S, Kawai S, Aoshima H, Kawamata O, Kawaguchi R, Hikiji K, Kato M, Iino S, Mizushima Y (1997) *Clin Diag Lab Immunol* 4:285–290.
13. Bumann D, Habibi H, Kan B, Schmid M, Goosmann C, Brinkmann V, Meyer TF, Jungblut PR (2004) *Infect Immunol* 72:6738–6742.
14. Obonyo M, Guiney DG, Harwood J, Fierer J, Cole SP (2002) *Infect Immun* 70:3295–3299.
15. Frucht DM, Fukao T, Bogdan C, Schindler H, O'Shea JJ, Koyasu S (2001) *Trends Immunol* 22:556–560.
16. Ferlazzo G, Munz C (2004) *J Immunol* 172:1333–1339.
17. Hafsi N, Voland P, Schwendy S, Rad R, Reindl W, Gerhard M, Prinz C (2004) *J Immunol* 173:1249–1257.
18. Lodolce JP, Boone DL, Chai S, Swain RE, Dassopoulos T, Trettin S, Ma A (1998) *Immunity* 9:669–676.
19. Kennedy MK, Glaccum M, Brown SN, Butz EA, Viney JL, Embers M, Matsuki N, Charrier K, Sedger L, Willis CR, *et al.* (2000) *J Exp Med* 191:771–780.
20. Ohteki T, Suzue K, Maki C, Ota T, Koyasu S (2001) *Nat Immunol* 2:1138–1143.
21. Cao X, Shores EW, Hu-Li J, Anver MR, Kelsall BL, Russell SM, Drago J, Noguchi M, Grinberg A, Bloom ET, *et al.* (1995) *Immunity* 2:223–238.
22. Yoshida H, Honda K, Shinkura R, Adachi S, Nishikawa S, Maki K, Ikuta K, Nishikawa SI (1999) *Int Immunol* 11:643–655.
23. Bode G, Mauch F, Malfertheiner P (1993) *Epidemiol Infect* 111:483–490.
24. Dunkley ML, Harris SJ, McCoy RJ, Musicka MJ, Eyers FM, Beagley LG, Lumley PJ, Beagley KW, Clancy RL (1999) *FEMS Immunol Med Microbiol* 24:221–225.
25. Ramarao N, Gray-Owen SD, Backert S, Meyer TF (2000) *Mol Microbiol* 37:1389–1404.
26. Nystrom J, Raghavan S, Svennerholm AM (2006) *Microbes Infect* 8:442–449.
27. Bergman MP, Engering A, Smits HH, van Vliet SJ, van Bodegraven AA, Wirth HP, Kapsenberg ML, Vandenbroucke-Grauls CM, van Kooyk Y, Appelmelk BJ (2004) *J Exp Med* 200:979–990.
28. Emilia G, Longo G, Luppi M, Gandini G, Morselli M, Ferrara L, Amarri S, Cagossi K, Torelli G (2001) *Blood* 97:812–814.
29. Velin D, Bachmann D, Bouzourene H, Michetti P (2005) *Gastroenterology* 29:142–155.
30. Jang MH, Kweon MN, Iwatani K, Yamamoto M, Terahara K, Sasakawa C, Suzuki T, Nochi T, Yokota Y, Rennert PD, *et al.* (2004) *Proc Natl Acad Sci USA* 101:6110–6115.
31. Hamada H, Hiroi T, Nishiyama Y, Takahashi H, Masunaga Y, Hachimura S, Kaminogawa S, Takahashi-Iwanaga H, Iwanaga T, Kiyono H, *et al.* (2002) *J Immunol* 168:57–64.
32. Khin MM, Hua JS, Ng HC, Wadstrom T, Bow H (2000) *World J Gastroenterol* 6:202–209.
33. De Vita S, Ferraccioli G, Avellini C, Sorrentino D, Dolcetti R, Di Loreto C, Bartoli E, Boiocchi M, Beltrami CA (1996) *Gastroenterology* 110:1969–1974.
34. Kroneld U, Jonsson R, Carlsten H, Bremell T, Johannessen AC, Tarkowski A (1998) *Scand J Rheumatol* 27:215–218.
35. Suzuki H, Duncan GS, Takimoto H, Mak TW (1997) *J Exp Med* 185:499–505.
36. Leder LD (1979) *Am J Dermatopathol* 1:39–42.
37. Lorenz RG, Chaplin DD, McDonald KG, McDonough JS, Newberry RD (2003) *J Immunol* 170:5475–5482.

Specific expression of hepatocyte nuclear factor-1β in the ovarian clear cell adenocarcinoma and its application to cytological diagnosis

Atsushi Higashiguchi,[1,2] Taketo Yamada,[1] Nobuyuki Susumu,[2] Taisuke Mori,[1] Atsushi Suzuki,[2] Daisuke Aoki[2] and Michiie Sakamoto[1,3]

Departments of [1]Pathology and [2]Obstetrics and Gynecology, Keio University School of Medicine, 35 Shinano-machi, Shinjuku-ku, Tokyo 160-8582 Japan

(Received September 25, 2006/Revised November 13, 2006/Accepted November 18, 2006/Online publication January 8, 2007)

Ascitic cytological diagnosis is critical, but ovarian adenocarcinoma cells and reactive mesothelial cells can be difficult to distinguish because they usually have atypical cell nuclei and increased nuclear/cytoplasmic ratios. Previous studies using DNA microarrays have demonstrated that hepatocyte nuclear factor-1β (HNF-1β) is expressed specifically in clear cell adenocarcinoma (CCC). Thus, in the present study, we investigated the usefulness of HNF-1β as an immunocytochemical diagnostic marker of CCC in ascitic specimens. We first confirmed that HNF-1β expression levels were significantly higher in CCC than in non-CCC (i.e. serous adenocarcinoma, mucinous adenocarcinoma and endometrioid adenocarcinoma) in 55 surgical specimens at both the mRNA ($P < 0.05$) and protein ($P < 0.05$) levels by real-time polymerase chain reaction and immunohistochemistry, respectively. Immunocytochemistry of 60 cytological specimens showed significant positivity in CCC cases whereas all non-CCC cells, except for three endometrioid adenocaricnoma cases, and mesothelial cells in the background stained negatively for anti-HNF-1β antibody ($P < 0.05$). The sensitivity and specificity were calculated to be 0.955 and 0.921, respectively. Immmunostaining patterns of HNF-1β on cytological specimens were similar to those observed on histopathological ovarian specimens from the same patients. Double immunohistochemical staining using anti-HNF-1β antibody and HBME-1, a mesothelium-specific monoclonal antibody, confirmed that anti-HNF-1β antibody distinguished CCC cells and mesothelial cells. In conclusion, our findings indicate the specific expression of HNF-1β in ovarian CCC and possible clinical applications of HNF-1β immunocytochemical staining for the differential cytopathological diagnosis of CCC from non-CCC, as well as from mesothelial cells using cytological specimens from ovarian carcinoma patients. (*Cancer Sci* 2007; 98: 387–391)

Ovarian adenocarcinomas have the worst prognosis of any gynecological carcinoma[1–3] because they are usually not detected until late, leading to dissemination in the abdominal peritoneum mediated by ascites.[4–6] The early detection of ovarian carcinoma is made difficult by a lack of symptoms,[7] other than abdominal distention caused by a huge ovarian mass and ascites. Sometimes, massive ascites is a solitary symptom lacking for primary tumors. Ascitic cytological diagnosis is very important in inoperable cases, recurrent cases and cases in which primary tumors are unclear.

Ovarian adenocarcinomas are classified into four major histological types on the basis of morphological criteria: serous adenocarcinoma, mucinous adenocarcinoma, endometrioid adenocarcinoma, and CCC.[8] CCC has a worse prognosis than any other ovarian carcinoma because of its low chemosensitivity,[9] even though it is usually detected at an early stage.[10] CCC is much more frequent among Japanese women than European and American women. CCC accounts for approximately 21% of ovarian adenocarcinomas in Japan and approximately 7.5% in most Western countries.[11]

The distinction of each pathological type on Papanicolaou-stained specimens is approached based on cytological features. However, cytological differential diagnosis between CCC cells and non-CCC cells is often difficult because floating cells in ascites are likely to be degenerated. Moreover, reactive mesothelial cells in ascites resemble adenocarcinoma cells in that they have obvious nucleoli, high mitotic rate, increased nuclear/cytoplasmic ratio with irregular chromatin clumping and vary in shape and size,[12–15] causing an indefinite diagnosis. Thus, an immunohistochemical marker in ascites would aid cytological diagnosis.

HNF-1β is a transcription factor that regulates the expression of liver-specific proteins such as albumin and α-fetoprotein in adult mammals and controls the growth and differentiation of the liver and kidney in the fetus.[16,17] We and Schwartz *et al.* previously revealed that HNF-1β is expressed at much higher levels in CCC than in other types of ovarian carcinoma by using a DNA microarray,[18,19] and have shown that HNF-1β is a potential immunohistochemical marker for surgical specimens.[18,20] Here we have examined the usefulness of HNF-1β as an immunocytochemical marker of CCC cells in ascites of ovarian carcinomas.

Materials and Methods

Clinical specimens. We evaluated 60 cytological specimens of malignant ascites arising from ovarian carcinomas (including 22 CCC, 24 serous adenocarcinomas, four mucinous adenocarcinomas and 10 endometrioid adenocarcinomas) from patients who underwent surgery at Keio University Hospital from 1995 to 2004; and 55 surgical specimens of ovarian carcinomas (including 21 CCC, 14 serous adenocarcinomas, eight mucinous adenocarcinomas and seven endometrioid adenocarcinomas) obtained from 2003 to 2005.

The final diagnosis of the histological type of ovarian carcinoma was based on histopathological and/or cytopathological findings. Histopathological features were as follows: for serous adenocarcinoma, malignant cells resembling epithelial cells of the ovitube and ovarian surface; for mucinous adenocarcinoma, tall, mucin-rich malignant cells resembling epithelial cells of the uterine endocervix and intestines; for endometrioid adenocarcinoma, endometrioid malignant cells; and for clear cell adenocarcinoma, glycogen-rich 'clear' cells and/or 'hobnail'-type cells whose nuclei projected to the cavity of the glands.[21] Cytopathological features were as follows: for serous adenocarcinoma, cells with a fairly high nuclear/cytoplasmic ratio and severely dysplatic

[3]To whom correspondence should be addressed. E-mail: msakamot@sc.itc.keio.ac.jp
Abbreviations: CCC, ovarian clear cell adenocarcinoma; DAB, 3,3′-diaminobenzidine, tetrahydrochloride; GAPDH, glyceraldehyde-3-phosphate dehydrogenase; HNF, hepatocyte nuclear factor; PBS, phosphate-buffered saline; PCR, polymerase chain reaction.

doi: 10.1111/j.1349-7006.2007.00398.x

nuclei forming small cell clusters because of loose connections; for mucinous adenocarcinoma, cells that are columnar and produce much mucin in the cytoplasm resulting in multiple vacuoles; for endometrioid adenocarcinoma, cells with mildly atypical nuclei and scanty cytoplasm forming large cell clusters resembling endometrial glands; for CCC, cells with a rich 'clear' cytoplasm containing glycogen and severely atypical nuclei with a few obvious nucleoli forming a 'mirror ball' pattern or raspberry body.[12–15]

The present study was approved by the ethics committee of the Keio University (Tokyo, Japan). All patients who underwent operations after 2003 were well informed and gave written consent for the investigations.

RNA extraction, reverse transcription and quantitative real-time PCR. The optimal cutting temperature compound-embedded frozen sections of surgically resected specimens were prepared, and one of the sections was stained with hematoxylin and eosin. According to the microscopic findings, the necrotic tissue and stroma were removed as thoroughly as possible. Total RNA was isolated from these frozen sections and cell lines using the ISOGEN Reagent (Wako Pure Chemical Industries, Japan) and contaminating genomic DNA was removed using DNaseI (Roche, Germany). Reverse transcription was done using a First-Strand cDNA Synthesis Kit (Amersham Biosciences, UK) with the random primer contained in the kit following the manufacturer's directions.

Quantitative real-time PCR analysis was carried out using the ABI PRISM 7000 Sequence Detection System (Applied Biosystems, USA) with SYBR remix Ex *Taq* (Takara Bio, Japan) according to the manufacturer's instructions. We used a PCR consisting of an initial denaturation at 94°C for 10 s, and 40 cycles of amplification at an annealing temperature of 60°C. The primer sequences used were as follows: human HNF-1β sense, 5′-GCCCACACACCA-CTTACTTCG-3′, and antisense, 5′-GTCCGTCAGGTAAGCAG-GGAC-3′; and human GAPDH sense, 5′-GAAGGTGAAGGTCG-GAGTC-3′, and antisense, 5′-GAAGATGGTGATGGGATTTC-3′. The *GAPDH* gene was the endogenous control for mRNA expression levels. Levels of mRNA in each tumor sample were normalized on the basis of the corresponding GAPDH level and recorded as a relative value. PCR amplification was carried out in triplicate for each sample.

Immunohistochemistry. The 10% formalin-fixed paraffin-embedded tissue was deparaffinized and rehydrated before it was autoclaved in citrate buffer (pH 7.0) for 10 min at 120°C and then incubated in 0.03% H_2O_2 in 95% methanol at room temperature for 20 min. After the slides were rinsed three times with PBS, blocking was carried out in the 1.5% normal rabbit serum for 30 min at room temperature. This was followed by incubation with an antihuman HNF-1β goat polyclonal antibody (sc-7411; Santa Cruz Biotechnology, USA) diluted 1:100 in 1% bovine serum albumin in PBS as a primary antibody at 4°C overnight. The slides were rinsed three times in PBS and incubated for 30 min with biotinylated rabbit antigoat immunoglobulin as the secondary antibody (Vector Laboratories, USA). Subsequently, they were incubated for 30 min with the avidin–biotin–peroxidase complex attached to a Vectastain ABC kit (Vector Laboratories). The slides were rinsed three times in PBS, then incubated for 5 min in DAB/Tris solution (three DAB/Tris tablets diluted in 150 mL distilled water; Muto Pure Chemicals, Japan) to which was added 15 μL of 30% H_2O_2. Finally, the slides were counterstained with Mayer's hematoxylin after three rinses in PBS.

Staining with the anti-HNF-1β antibody in the cell nuclei was classified into six grades (≥75%, 5; 51–75%, 4; 26–50%, 3; 6–25%, 2; 1–5%, 1; ≤1%, 0). More than 100 cancer cells were counted. Nuclei that were stained strongly and recognizable microscopically even at low power were judged as positive. Faint staining that was barely recognized at low power was judged as negative.

Immunocytochemistry. Malignant ascites freshly removed from 2003 to 2004 was centrifuged and the supernatant was discarded. The rest was resolved with 10 mL PBS and further processed by Ficoll (IBL, Japan) and centrifuged onto microscopic slides. The slides were then dried and the cells were placed on them before being fixed with 95% ethanol. The archival (1995–2002) cytological slides with Papanicolaou's staining were decolorized in a mixture of 1% hydrogen chloride and 70% ethanol overnight.

All cytological specimens mentioned above were boiled for 10 min in citrate buffer (pH 7.0). After cooling at room temperature, the slides were rinsed with PBS. Blocking and staining were carried out as described above. The slides were then incubated for 5 min in a DAB/Tris solution containing 15 μL of 30% H_2O_2, 97.5 mg sodium azide and 1.35 g sodium chloride. Finally, the slides were counterstained with Mayer's hematoxylin after being rinsed three times in PBS. Staining of the cytological specimens was classified in the same manner as the surgical specimens mentioned above.

Double immunocytochemical staining using anti-HNF-1β antibody and HBME-1 (DAKO, USA), a mesothelium-specific monoclonal antibody,[21] a Histofine New Fuchsin Substrate Kit (Nichirei Corporation, Japan), and Fast Blue RR Salt (Sigma Chemicals, USA) for color developing, were carried out on both ascitic cytological specimens of patients with CCC and 1:100 mixed-cell samples of a CCC-derived cell line, and mesothelial cells.

Mesothelial cells and a CCC cell line. Separation of the mesothelial cells from resected omentum was done according to a method described previously.[22] All cells were used at passages 2–5. RMG-I cell lines, established previously from ascites of a patient with CCC in our laboratory,[23] were cultured in F-12 supplemented with 10% fetal bovine serum, 100 IU/mL ampicillin, and 100 μg/mL streptomycin in a humidified atmosphere of 5% CO_2 and 95% air at 37°C.

Statistical analysis. We analyzed all of the data using the Statcel statistical program (OMC, Japan), then evaluated the statistical significance using Mann–Whitney's *U*-test. We considered $P < 0.05$ to be statistically significant.

Results

Expression of HNF-1β in surgical specimens. We first examined the expression of HNF-1β mRNA in human ovarian carcinoma tissues using quantitative real-time PCR in order to confirm the specific expression of HNF-1β in CCC. Figure 1 shows the relationship between the relative expression of HNF-1β mRNA normalized to that of GAPDH and histological types of ovarian carcinomas. In 21 CCC, nine (36.7%) were given HNF-1β : GAPDH mRNA ratios of 3.0 or higher, whereas all 14 serous adenocarcinomas, eight mucinous adenocarcinomas and 12 endometrioid adenocarcinomas were given HNF-1β : GAPDH mRNA ratios of lower than 3.0. Four (19.0%) CCC and four (33.3%) endometrioid adenicarcinomas were given HNF-1β : GAPDH mRNA ratios of 1.0 through 3.0. A significant difference was recognized between CCC (4.00 ± 5.38) and non-CCC (0.38 ± 0.69) ($P < 0.01$ or $P < 0.05$ by Mann–Whitney's *U*-test) similar to the data obtained with the DNA microarray described previously.[18]

The immunohistochemical expression of HNF-1β on formalin-fixed paraffin-embedded histological specimens of patients whose fresh-frozen tissue was used in the above quantitative real-time PCR analysis was then examined (Fig. 2). The same trend was recognized in both the immunohistochemical and mRNA expression of HNF-1β. That is, in 21 CCC cases, 10 (47.6%) were given a score of 4 or 5, five (23.8%) were given a score of 2 or 3, and only six (28.6%) were given a score of 0 or 1, whereas 14 serous adenocarcinomas and eight mucinous adenocarcinomas were always

doi: 10.1111/j.1349-7006.2007.00398x

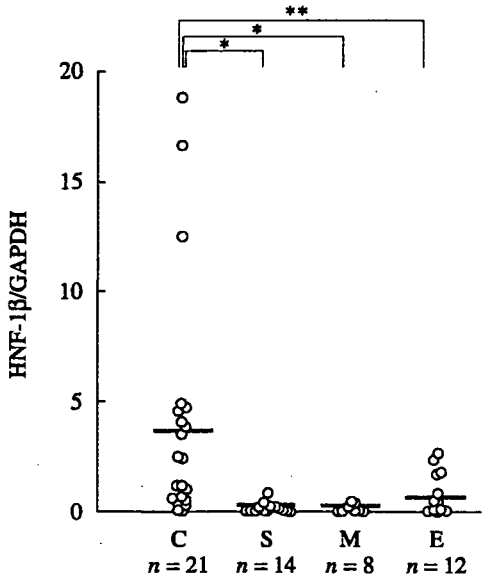

Fig. 1. Relative expression of hepatocyte nuclear factor-1β (HNF-1β) mRNA. Levels of HNF-1β mRNA in 55 ovarian carcinoma specimens (C, clear cell adenocarcinoma, $n = 21$; E, endometrioid adenocarcinoma, $n = 12$; M, mucinous adenocarcinoma, $n = 8$; S, serous adenocarcinoma, $n = 14$) were normalized with human glyceraldehyde-3-phosphate dehydrogenase expression. The bars indicate the average expression level of HNF-1β in each group. A significant difference was recognized between ovarian clear cell adenocarcinomas (CCC) and each type of non-CCC. $*P < 0.01$, $**P < 0.05$; by Mann–Whittney's *U*-test.

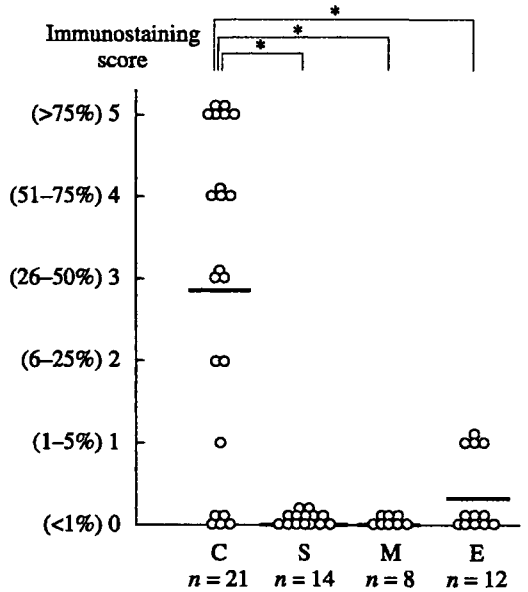

Fig. 2. Hepatocyte nuclear factor-1β (HNF-1β) immunostaining scores of surgical specimens. Specimens from the same patients ($n = 55$) as in Fig. 1 (C, clear cell adenocarcinoma, $n = 21$; E, endometrioid adenocarcinoma, $n = 12$; M, mucinous adenocarcinoma, $n = 8$; S, serous adenocarcinoma, $n = 14$) were analyzed. Each specimen was classified according to the percentage of cells with positive nuclei. The bars indicate the average score for each group. The immunostaining scores for ovarian clear cell adenocarcinomas were significantly higher than those for other histologies. $*P < 0.01$; by Mann–Whittney's *U*-test.

given a score of 0. Of 12 endometrioid adenocarcinomas, four and eight were given scores of 1 and 0, respectively. The immunostaining scores for CCC were significantly higher than those for other histologies ($P < 0.01$ by Mann–Whitney's *U*-test). Because these

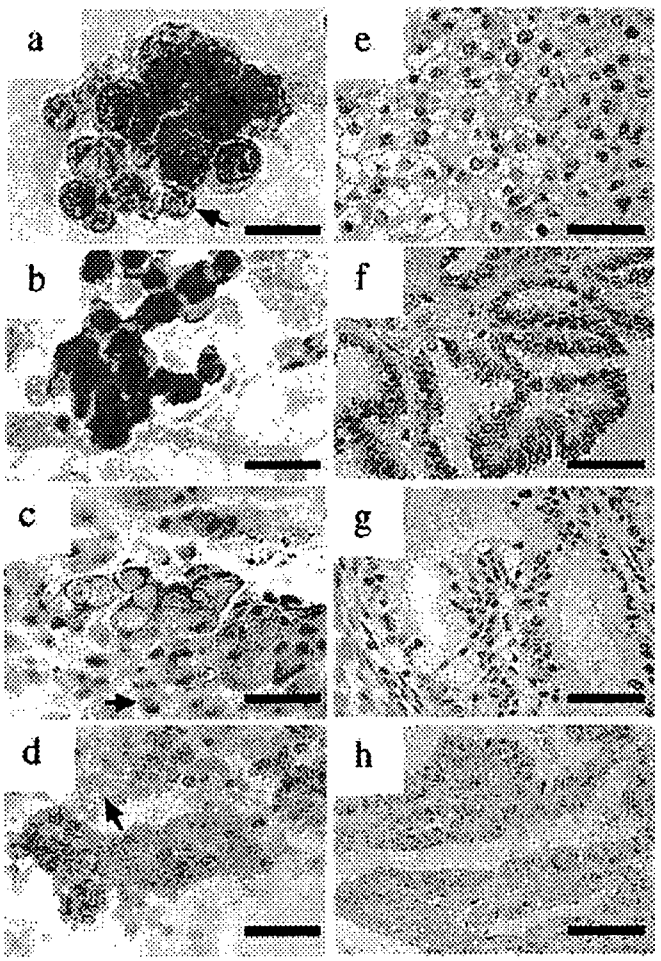

Fig. 3. Immunostaining of ascitic and surgical specimens using anti-hepatocyte nuclear factor-1β (HNF-1β) antibody. The ascitic cytological (a–d) and surgical (e–h) specimens from four patients with ovarian clear cell adenocarcinoma (a,e), serous adenocarcinoma (b,f), mucinous adenocarcinoma (c,g) and endometrioid adenocarcinoma (d,h) are shown. Anti-HNF-1β antibody showed positive staining for only the cell nuclei of ovarian clear cell adenocarcinomas, and not those of serous adenocarcinoma, mucinous adenocarcinoma or endometrioid adenocarcinoma. Representative mesothelial cells in the slides of ascitic cytological specimens are indicated with arrows (a,c,d). Scale bar: (a–c) 50 μm; (d–h) 100 μm.

scores were variables of category, they need not compare mean values of these scores between CCC and non-CCC.

Expression of HNF-1β protein in cytological specimens. In order to assess the usefulness of the application of HNF-1β on cytological specimens, immunocytochemistry was carried out. Specimens from 17 cases were used for both immunocytochemistry and immunohistochemistry. Similarly to the surgical specimens, HNF-1β was expressed diffusely in the nuclei of cytological specimens of CCC but not in those of non-CCC (Fig. 3). The immunohistochemical and immunocytochemical scores in the same case did not always give the same score; however, a significant correlation was shown by Spearman's rank correlation test between the scores of immunohistochemistry and immunocytochemistry in the 17 cases ($P < 0.01$; correlation rate = 0.94). In total, 60 cases were analyzed and anti-HNF-1β antibody stained only the cell nuclei in CCC in the ascitic cytological specimens, except in three cases of endometrioid adenocarcinoma in which anti-HNF-1β antibody stained focally in the nuclei (Fig. 4). In all 60 cases, more than

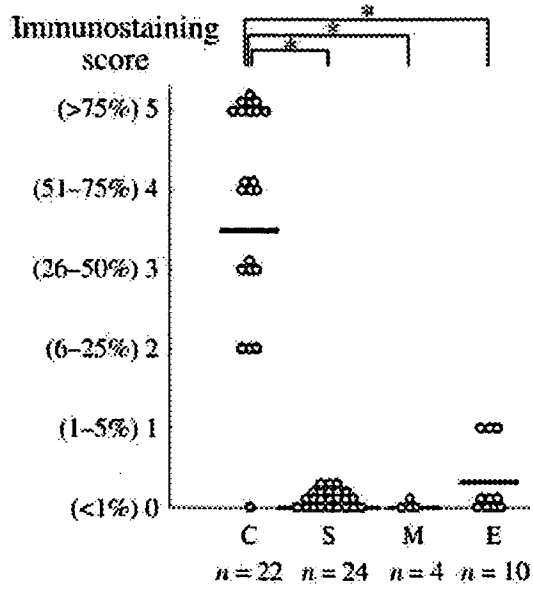

Fig. 4. Hepatocyte nuclear factor-1β (HNF-1β) immunostaining scores of ascitic cytological specimens. The specimens arising from patients ($n = 60$) with ovarian carcinomas (C, clear cell adenocarcinoma, $n = 22$; E, endometrioid adenocarcinoma, $n = 10$; M, mucinous adenocarcinoma, $n = 4$; S, serous adenocarcinoma, $n = 24$) were analyzed. Each specimen was classified according to the percentage of cells with positive nuclei. The bars indicate the average score for each group. The immunostaining scores for ovarian clear cell adenocarcinomas were significantly higher than those for other histologies. $^{*}P < 0.05$, $^{**}P < 0.01$; by Mann–Whittney's *U*-test).

100 mesothelial cells for each case were examined and no cells were stained by the antibody (Fig. 3). Of 22 CCC, 21 (95.5%) showed score 2 or higher whereas 24 serous adenocarcinomas and four mucinous adenocarcinomas, and 10 endometrioid adenocarcinomas always showed score 0 or 1. The immunostaining scores for CCC (3.46 ± 1.69) were significantly higher than those for other histologies (0.08 ± 0.28) ($P < 0.05$ by Mann–Whitney's *U*-test; Fig. 4). Because the five percentile of the immunostaining scores for CCC was 0.08 and the 95 percentile of the immunostaining scores for non-CCC was 0.64, the HNF-1β immunostaining score 0 was defined as negative and score 1 and over were defined as positive. According to the definition, the sensitivity and specificity were calculated as 0.955 and 0.921, respectively.

Differentiating between CCC and mesothelial cells. In order to confirm the *in vivo* findings of clinical cases, we conducted an *in vitro* analysis using CCC and mesothelial cells. Anti-HNF-1β antibody stained the nuclei of CCC cells but not mesothelial cells, whereas mesothelial cells were stained by the HBME-1 antibody in the cytoplasm. The same reciprocal pattern of staining was observed in the clinical cytological specimens of CCC patients with double immunostaining (Fig. 5).

Discussion

In the present study, we first confirmed the specific expression of HNF-1β in CCC in surgical specimens using real-time quantitative PCR and immunohistochemistry. The results were consistent with previous findings based on immunohistochemistry.[18,20] At present, the potential causes of the overexpression of HNF-1β in CCC are not clear. Hirasawa *et al.* demonstrated the amplification of 17q21–24 in 40% (8/20) of CCC cases using the comparative genomic hybridization technique.[24] Because HNF-1β is located at 17cen-17q23, this amplification might upregulate its expression. Terasawa *et al.* carried out methylation profiling of HNF-1β among cases of ovarian carcinomas and revealed epigenetic deletions of HNF-1β in 41.4% of serous adenocarcinoma cases, 25.0% of mucinous adenocarcinoma cases, 28.6% of endometrioid adenocarcinoma cases and 0% of CCC cases.[25] This epigenetic mechanism also might contribute to HNF-1β expression in CCC.

HNF-1β expression was closely related to histological type based on morphological features, though the function of HNF-1β in CCC is not clear. Cheng *et al.* reported that homeobox genes, which have a homeodomain just like HNF-1β, played pivotal roles in the peculiar histology of ovarian epithelial adenocarcinomas except CCC.[26] HNF-1β has been reported to act antagonistically toward HNF-1α,[27] which increases expression of sodium-glucose cotransporter 1,[28] glucose 6-phosphate transporter, and glucose 6-phosphatase.[29] Given that glycogen storage was shown in the hepatocytes of HNF-1α-null and mutant,[29,30] HNF-1β overexpression might cause clear cytoplasm characteristics. In addition, we previously reported that HNF-1β might associate with an antiapoptotic function of CCC.[18]

We further assessed the usefulness of the application of HNF-1β to cytological specimens by immunocytochemistry. In 17 cases that were used for both immunohistochemistry and immunocytochemistry, similar staining with the anti-HNF-1β antibody was demonstrated in both cytological specimens and surgical specimens of the same patient. Similar to the results for surgical specimens, the majority of cytological specimens of CCC cases were classified with a score of 4 and 5, whereas all non-CCC cases

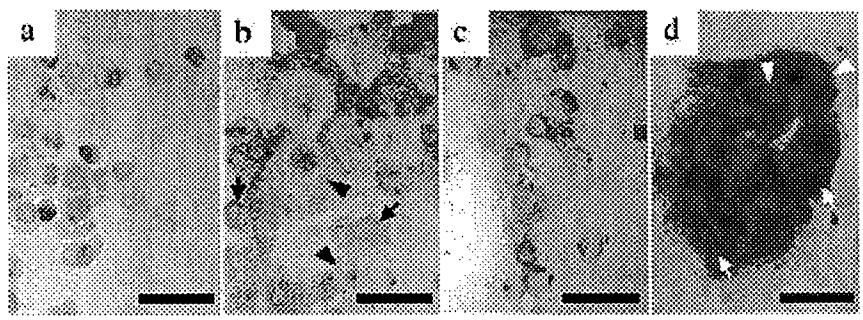

Fig. 5. Immunochemical discrimination between ovarian clear cell adenocarcinoma cells and mesothelial cells. The cytospin of (a) RMG-I cells, (c) mesothelial cells and (b) a mixture of RMG-I cells and mesothelial cells were subjected to double immunocytochemical staining using anti-hepatocyte nuclear factor-1β (HNF-1β) antibody (brown color) and HBME-1 (blue color). HNF-1β was positive only in the cell nuclei of RMG-I in which HBME-1 is negative in the cytoplasm. (d) In the ascitic specimens from a ovarian clear cell adenocarcinoma (CCC) patient, HBME-1 was negative in the cytoplasm of CCC cells and HNF-1β was positive in the CCC cell nuclei, whereas HNF-1β was negative in the nuclei of the mesothelial cells. Representative CCC cells and mesothelial cells are indicated by arrowheads and arrows, respectively. Scale bar: 50 μm.

doi: 10.1111/j.1349-7006.2007.00398x

except three endometrioid adenocarcinoma cases were stained negatively. Thus, HNF-1β could be applied to clinical cytological diagnosis as a molecular marker. To our knowledge, HNF-1β is the first histology-type-specific cytological diagnostic marker. HNF-1β also stained negatively not only the stroma of paraffin-embedded cancer tissue but also the mesothelial cells in cytological specimens. Double immunocytochemical staining using HBME-1[21] and anti HNF-1β antibody revealed a clear distinction between CCC cells and mesothelial cells. Diverse markers are applied to ascitic and pleural effusion cytology for specific recognition of cancer cells from mesothelial cells. Ber-EP4, B72.3, anticarcinoembryonic antigen antibody, anti-CA125 antibody, antiepithelial membrane antigen and LeuM1 are markers sensitive to cancer cells,[31-33] whereas HBME-1[21] and calretinin[34] are applied as mesothelium-sensitive markers. In ovarian cancer, a novel monoclonal antibody,[35] a combination of Ber-EP4 and calretinin, and so forth,[36,37] had been applied. We consider HNF-1β applicable to clinical specimens, and evaluations of the sensitivity and specificity of the above-mentioned markers to be necessary.

In conclusion, our results indicated specific expression of HNF-1β in ovarian CCC in both neoplastic tissues and ascites and suggest that HNF-1β can be applied as a CCC-specific immunocytochemical marker of ascites. For the purpose of clinical application, it is necessary to assume the usefulness of HNF-1β prospectively.

Acknowledgments

This work was supported in part by a Grant-in-Aid for Scientific Research on Priority Areas 'Cancer' and for the 21st Century Center of Excellence program from the Ministry of Education, Science, Sports and Culture of Japan, for the Third Term Comprehensive 10-Year Strategy for Cancer Control from the Ministry of Health and Welfare of Japan. The authors thank Dr Nao Suzuki (Department of Obstetrics and Gynecology, St Marianna University School of Medicine, Kawasaki, Japan) for encouragement during the early days of the study and Dr Yutaka Tamada (Department of Obstetrics and Gynecology, Keio University School of Medicine, Tokyo, Japan) for providing of peritoneal mesothelial cells.

References

1 Landis SH, Murray T, Bolden S, Wingo PA. Cancer statistics, 1999. *CA Cancer J Clin* 1999; **49**: 8–31.
2 Holschneider CH, Berek JS. Ovarian cancer: epidemiology, biology, and prognostic factors. *Semin Surg Oncol* 2000; **19**: 3–10.
3 Boyle P, Maisonneuve P, Autier P. Towards cancer control in women. *J Epidemiol Biostat* 1998; **3**: 137–68.
4 Berek JS, Hacker NF. *Practical Gynecologic Oncology*, 3rd edn. Philadelphia: Lippincott, Williams & Wilkins, 2000.
5 Goff BA, Mandel LS, Muntz HG, Melancon CH. Ovarian cancer diagnosis: results of a national ovarian cancer survey. *Cancer* 2000; **89**: 2068–75.
6 Olson SH, Mignone L, Nakraseive C, Caputo TA, Barakat RR, Harlap S. Symptoms of ovarian cancer. *Obstet Gynecol* 2001; **98**: 212–17.
7 Smith EM, Anderson B. The effects of symptoms and delay in seeking diagnosis on stage of disease at diagnosis among women with cancers of the ovary. *Cancer* 1985; **56**: 2727–32.
8 Lee KR, Russell P, Tavassoli FA, *et al.* Surface epithelial stromal tumors. In: Tavassoli FA, Devilee P, eds. *WHO Classification of Tumors. Pathology and Genetics of Tumors of the Breast and Female Genital Organs*. Lyon: IARC Press, 2003; 117–145.
9 Enomoto T, Kuragaki C, Yamasaki M *et al.* Is clear cell carcinoma and mucinous carcinoma of the ovary sensitive to combination chemotherapy with paclitaxel and carboplatin? *Proc Am Soc Clin Oncol* 2003; **22**: 447.
10 O'Brien MER, Schofield JB, Tan S, Fryatt I, Fisher C, Wiltshaw E. Clear cell epithelial ovarian cancer (mesonephroid): bad prognosis only in early stages. *Gynecol Oncol* 1993; **49**: 250–4.
11 Seidman JD, Russell P, Kurman RJ. Surface epithelial tumors of the ovary. In: Kurman RJ, ed. *Blaustein's Pathology of the Female Genital Tract*, 5th edn. New York: Springer-Verlag, 2002, 791–804.
12 Kocjan G. *Atras of Diagnostic Cytopathology*, 2nd edn. New York: Churchill Livingstone, 1997.
13 Atahan S, Ekinci C, Icli F, Erdogan N. Cytology of clear cell carcinoma of the female genital tract in fine needle aspirates and ascites. *Acta Cytol* 2000; **44**: 1005–9.
14 Ito H, Hirasawa T, Yasuda M, Osamura RY, Tsutsumi Y. Excessive formation of basement membrane substance in clear-cell carcinoma of the ovary: diagnostic value of the 'raspberry body' in ascites cytology. *Diagn Cytopathol* 1997; **16**: 500–4.
15 Laucirica R, Schultenover SJ. Body cavity fluids. In: Ramzy I, ed. *Clinical Cytopathology and Aspiration Biopsy*, 2nd edn. New York: McGraw-Hill; 2005: 205–25.
16 Bohn S, Thomas H, Turan G *et al.* Distinct molecular and morphogenetic properties of mutations in the human HNF1β gene that lead to defective kidney development. *J Am Soc Nephrol* 2003; **14**: 2033–41.
17 Coffiner C, Gresh L, Fiette L *et al.* Bile system morphogenesis defects and liver dysfunction upon targeted deletion of HNF1β. *Development* 2002; **129**: 1829–38.
18 Tsuchiya A, Sakamoto M, Yasuda J *et al.* Expression profiling in ovarian clear cell carcinoma: identification of hepatocyte nuclear factor-1β as a molecular marker and a possible molecular target for therapy of ovarian clear cell carcinoma. *Am J Pathol* 2003; **163**: 2503–12.
19 Schwartz DR, Kardia SL, Shedden KA *et al.* Gene expression in ovarian cancer reflects both morphology and biological behavior, distinguishing clear cell from other poor-prognosis ovarian carcinomas. *Cancer Res* 2002; **62**: 4722–9.
20 Kato N, Sasou S, Motoyama T. Expression of hepatocyte nuclear factor-1β (HNF-1β) in clear cell tumors and endometriosis of the ovary. *Mod Pathol* 2006; **19**: 83–9.
21 Sheibani K, Esteban JM, Bailey A, Battifora H, Weiss LM. Immunopathologic and molecular studies as an aid to the diagnosis of malignant mesothelioma. *Hum Pathol* 1992; **23**: 107–16.
22 Tamada Y, Iida S, Aoki D, Nozawa S, Irimura T. Carbohydrate epitopes and mucins expressed by 17 human ovarian carcinoma cell lines. *Oncol Res* 1999; **11**: 233–41.
23 Nozawa S, Tsukazaki K, Sakayori M, Jeng CH, Iizuka R. Establishment of a human ovarian clear cell adenocarcinoma cell line (RMG-I) and its single cell cloning – With special reference to the stem cell of the tumor. *Hum Cell* 1988; **1**: 426–35.
24 Hirasawa A, Saito-Ohara F, Inoue J *et al.* Association of 17q21-q24 gain in ovarian clear cell adenocarcinomas with poor prognosis and identification of PPM1D and APPBP2 as likely amplification targets. *Clin Cancer Res* 2003; **9**: 1995–2004.
25 Terasawa K, Toyota M, Sagae S *et al.* Epigenetic inactivation of TCF2 in ovarian cancer and various cancer cell lines. *Br J Cancer* 2006; **94**: 914–21.
26 Cheng W, Liu J, Yoshida H, Rosen D, Naora H. Lineage infidelity of epithelial ovarian cancers is controlled by *HOX* genes that specify regional identity in the reproductive tract. *Nat Med* 2005; **11**: 531–7.
27 Vallet V, Bens M, Antoine B *et al.* Transcription factors and aldolase B gene expression in microdissected renal proximal tubules and derived cell lines. *Exp Cell Res* 1995; **216**: 363–70.
28 Rhoads DB, Rosenbaum DH, Unsal H, Isselbacher KJ, Levitsky LL. Circadian periodicity of intestinal Na+/glucose cotransporter1 mRNA levels is transcriptionally regulated. *J Biol Chem* 1998; **273**: 9510–16.
29 Lee YH, Magnuson MA, Muppala V, Chen SS. Liver-specific reactivation of the inactivated *Hnf-1α* gene. Elimination of liver dysfunction to establish a mouse MODY3 model. *Mol Cell Biol* 2003; **23**: 923–32.
30 Hiraiwa H, Pan CJ, Lin B, Akiyama TE, Gonzalez FJ, Chou JY. A molecular link between the common phenotypes of type 1 glycogen storage diasease and HNF-1β-null mice. *J Biol Chem* 2001; **276**: 7963–7.
31 Shield PW, Callan JJ, Devine PL. Markers for metastatic adenocarcinoma in serous effusion specimens. *Diagn Cytopathol* 1994; **11**: 237–45.
32 Dejmek A, Hjerpe A. Reactivity of six antibodies in effusions of mesothelioma, adenocarcinoma and mesotheliosis: stepwise logistic regression analysis. *Cytopathology* 2000; **11**: 8–17.
33 Davidson B, Risberg B, Kristensen G *et al.* Detection of cancer cells in effusions from patients diagnosed with gynaecological malignancies. Evaluation of five epithelial markers. *Virchows Arch* 1999; **435**: 43–9.
34 Barberis MC, Faleri M, Veronese S, Casadio C, Viale G. Calretinin: A selective marker of normal and neoplastic mesothelial cells in serous effusions. *Acta Cytol* 1997; **41**: 1757–61.
35 McCluggage WG, Maxwell P, Veenstra H, Frick CE, Laeng RH, Tiltman AJ. Monoclonal antibody SM047 as an immunohistochemical marker of ovarian adenocarcinoma. *Histopathol* 2001; **38**: 542–9.
36 Sato S, Okamoto S, Ito K, Konno R, Yajima A. Differential diagnosis of mesothelial and ovarian cancer cells in ascites by immunocytochemistry using Ber-EP4 and calretinin. *Acta Cytol* 2000; **44**: 485–8.
37 Okamoto S, Ito K, Sasano H. Ber-EP4 and anti-calretinin antibodies: a useful combination for differential diagnosis of various histological types of ovarian cancer cells and mesothelial cells. *Tohoku J Exp Med* 2005; **206**: 31–40.

bjh research paper

Establishment of a novel childhood acute myeloid leukaemia cell line, KOPM-88, containing partial tandem duplication of the *MLL* gene and an *in vivo* model for childhood acute myeloid leukaemia using NOD/SCID mice

Mutsumi Hayashi,[1,2] Kensuke Kondoh,[1,3] Yuji Nakata,[1,4] Akitoshi Kinoshita,[3] Taijiro Mori,[5] Takao Takahashi,[1] Michi-ie Sakamoto[2] and Taketo Yamada[2]

[1]Department of Pediatrics, Keio University School of Medicine, [2]Department of Pathology, Keio University School of Medicine, Tokyo, [3]Department of Pediatrics, St Marianna University School of Medicine, Kanagawa, Japan, [4]Division of Hematology/Oncology, Department of Medicine, University of Pennsylvania School of Medicine, Philadelphia, PA, USA, and [5]Mori Children's Clinic, Saitama, Japan

Received 29 November 2006; accepted for publication 31 January 2007

Correspondence: Mutsumi Hayashi, MD, Department of Pediatrics, Keio University School of Medicine, 35 Shinano-machi, Shinjuku-ku, Tokyo 160–8582, Japan.
E-mail: mutsumi@mtb.biglobe.ne.jp

Summary

MLL gene rearrangement is common in both adult and childhood acute myeloid leukaemia (AML), and its role in oncogenesis has been investigated. While over 50 translocated-partner genes have been identified so far, few studies have detailed the molecular mechanism of partial tandem duplication (PTD) of the *MLL* gene. The prognostic impact and contribution to leukaemogenesis of *MLL*-PTD, especially in childhood cases, remain unknown. We have established a novel cell line containing *MLL*-PTD derived from an 11-year-old patient with AML and designated as KOPM-88. KOPM-88 cells exhibited certain characteristics associated with the myeloid lineage including abundant primary granules in the cytoplasm and the expression of myeloperoxidase. The cell growth of KOPM-88 was cytokine independent but was accelerated by granulocyte colony-stimulating factor and granulocyte-macrophage colony-stimulating factor. *MLL*-PTD of exon 2 to exon 6 and exon 2 to exon 8 was revealed using Southern blotting, fluorescence *in situ* hybridisation, and reverse transcription polymerase chain reaction/DNA sequencing. Furthermore, non-obese diabetic/severe combined immunodeficient mice inoculated with KOPM-88 cells exhibited leukaemic infiltrations in the bone marrow and hemiparalysis because of compression myelopathy. This is the first report of an *in vivo* animal model exhibiting the systemic involvement of childhood AML containing *MLL*-PTD. KOPM-88 cells and our murine model may be useful for investigating the pathogenesis of childhood AML associated with *MLL* gene rearrangement.

Keywords: cell line, *MLL* gene, partial tandem duplication, childhood acute myeloid leukaemia, animal model.

Acute myeloid leukaemia (AML) accounts for approximately 17% of childhood acute leukaemia (Hall, 2001). Despite advances in high-dose chemotherapy and stem cell transplantation, the prognosis of childhood AML is still poorer than that of acute lymphoblastic leukaemia (ALL) (Goubin *et al*, 2006). The prognostic factors for childhood AML have been studied for therapy modified by various risk groups. A subclassification of FAB M5, an age of older than 10 years, and some chromosomal abnormalities have been related to a poorer prognosis (Chang *et al*, 2000; Razzouk *et al*, 2006). As for cytogenetic characteristics, patients with inv(16) and t(8;21) have a favourable outcome, while patients with other chromosomal abnormalities like a 11q23 abnormality have a poor prognosis (Raimondi *et al*, 1999). Alterations of *MLL* gene (Ziemin-van der Poel *et al*, 1991) located on 11q23 are common genetic abnormalities in both ALL and AML. Though more prevalent in infant leukaemia, alterations of *MLL* gene have been reported for all age groups. *MLL* gene rearrangement results in the production of aberrant proteins, and aberrant MLL proteins are considered to have important roles

  doi:10.1111/j.1365-2141.2007.06553.x

in leukaemogenesis. The MLL protein is a homeotic regulator that positively regulates the maintenance of the homeotic (Hox) gene, thought to be important for appropriate haematopoietic development (Li *et al*, 2005). In ALL, *MLL* gene rearrangements are found in about 6% of paediatric cases, about 7% of adult cases, and up to 70–80% of infant cases. The most common translocation involving *MLL* in ALL is t(4;11) in all age groups (The Groupe Francais de Cytogenetique Hematologique, 1996; Pais *et al*, 2005; Luciani *et al*, 2006). Although t(4;11) ALL is well known to have a poor prognosis, recent studies suggest the prognosis of cases with *MLL* rearrangements other than t(4;11) is as poor as that of the t(4;11) cases in all age groups (The Groupe Francais de Cytogenetique Hematologique, 1996; Pais *et al*, 2005). In AML, *MLL* rearrangements are found in 10–24% of paediatric cases, 10–15% of adult cases, and up to 60–70% of infant cases (Munoz *et al*, 2003; Palle *et al*, 2005; Luciani *et al*, 2006; Shih *et al*, 2006). The most common translocation involving *MLL* in AML is t(9;11) in all age groups (Pui *et al*, 2000; Shih *et al*, 2006). The prognostic impact of *MLL* rearrangement on AML cases remains controversial because of different treatment protocols among the study groups. Many studies have suggested a poor prognosis for cases with *MLL* rearrangements (Munoz *et al*, 2003), but others have reported no significant difference between cases with and those without *MLL* rearrangements (Pui *et al*, 2000). Recent studies reported favourable outcomes in cases with AML containing t(9;11) compared to cases with *MLL* rearrangements other than t(9;11), because of the high sensitivity of these patients to Cytarabine (Pui *et al*, 2000; Palle *et al*, 2005).While translocations with more than 50 partner genes have been identified to date (Basecke *et al*, 2006), few studies have examined new *MLL* rearrangements, such as partial tandem duplications (PTDs) (Schichman *et al*, 1994), which are undetectable using conventional cytogenetics. PTDs are found in 5–20% of adult AML cases with normal karyotype and 25–54% of cases with trisomy 11 (Basecke *et al*, 2006). In adult cases, AML with *MLL*-PTD has been reported to have a poorer prognosis than AML cases without *MLL* rearrangements (Dohner *et al*, 2002; Munoz *et al*, 2003; Mitterbauer-Hohendanner & Mannhalter, 2004), but the prognosis was not significantly different when compared to that of cases with other *MLL* rearrangements (Shih *et al*, 2006). Although the prognosis of AML with *MLL*-PTD in paediatric and infant cases is also reported to be worse than cases without *MLL*-PTD, the frequency and the prognosis of patients with *MLL*-PTD compared with other *MLL* aberrations among paediatric and infant AML are controversial because of the limited number of studied cases (Shiah *et al*, 2002; Basecke *et al*, 2006). The most common section involved in *MLL*-PTDs is exon 2 to exon 6 (exon 3 to exon 7 by the new nomenclature of Basecke *et al*, 2006) followed by exon 2 to exon 8 (exon 3 to exon 11 by new nomenclature) and exon 2 to exon 7 (exon 3 to exon 10 by new nomenclature), and combinations of alternatively spliced products are frequently observed (Yu *et al*, 1996; Shiah *et al*, 2002; Shih *et al*, 2006).

To improve our understanding of the pathobiology of childhood AML, an *in vivo* animal model for the disease is needed. The non-obese diabetic severe combined immunodeficient (NOD/SCID) mouse strain was bred in the late 1990s; this strain proved to be a better host for human haematopoietic cells than SCID mice. NOD/SCID mice lack functional T and B lymphocytes, are missing a haemolytic complement pathway, and have depressed natural killer (NK) cell activity (Shultz *et al*, 1995). As the first ALL animal model was reported (Kamel-Reid *et al*, 1989) in which the ALL cell line A-1 was transplanted in a SCID mouse, many ALL cell lines have been engrafted in immunodeficient mice to induce a leukaemic state; the resulting *in vivo* ALL models have been widely used. On the other hand, while 70% of AML blast cells from patients are reported to engraft and infiltrate the bone marrow of NOD/SCID mice (Ailles *et al*, 1999), the numbers in AML animal models using established cell lines are limited. As for AML cell lines with *MLL* gene rearrangement, eleven cell lines with *MLL* translocation, four with PTDs, and three with amplification have been reported so far (Drexler *et al*, 2004). Among the four cell lines with PTD of the *MLL* gene, only one cell line (EOL-1, established from an adult with eosinophilic leukaemia), has been engrafted in NOD/SCID mice (Saito *et al*, 1985; Drexler *et al*, 2004; Henschler *et al*, 2005). To date, no animal model for childhood AML characterised by *MLL* gene rearrangement has been established.

We formerly reported a paediatric case of AML with hypergranular cytoplasm accompanied by a rearrangement of the *MLL* gene, who also exhibited severe disseminated intravascular coagulation (DIC) (Nakata *et al*, 1999). In the present study, we established a novel cell line, KOPM-88, from this patient's peripheral blood, and investigated its cellular characteristics, including its lineage and *MLL* gene structure. In our previous study, we reported that the patient's blasts exhibited a t(X;11)(q24;23) translocation, but further study of the KOPM-88 cells revealed PTD of the *MLL* gene, but no translocation. Here, we also report the engraftment of KOPM88 cells into NOD/SCID mice to establish an *in vivo* animal model for childhood AML.

Materials and methods

Case report

The KOPM-88 cell line was established from an 11-year-old Japanese boy with relapsed AML. At the time of his initial diagnosis, the patient received chemotherapy that included doxorubicin, cytosine arabinoside, methotrexate, vincristine and 6-mercaptopurine (but not topoisomerase II inhibitors), and achieved a complete remission. However, he relapsed 5 years after his initial diagnosis and died 2 years after the relapse. At the time of both initial diagnosis and relapse, coagulation studies indicated severe disseminated intravascular coagulation (DIC). Both the primary and relapsed leukaemic cells exhibited abundant granules but without Auer bodies.

The primary leukaemic cells were positive for myeloperoxidase (MPO), CD4 and CD13, and negative for HLA-DR, CD33, CD11b; at relapse, cells were positive for MPO, CD4, CD13 and CD33 and negative for HLA-DR, CD34, CD11b and CD56. The representative karyotype of the bone marrow cells at relapse was 46XY, t(X;11)(q24;q23). Southern blot analysis showed an *MLL* gene rearrangement but no *RARA* gene rearrangement in the leukaemic cells at the time of the relapse (previously reported by Nakata *et al*, 1999).

Cell cultures

A heparinised peripheral blood sample was obtained from the patient at the time of his relapse, following informed consent. Mononuclear cells were separated out using Ficoll-Conray gradient centrifugation. After washing, the mononuclear cells were seeded in RPMI 1640 tissue culture medium (Sigma-Aldrich, St. Louis, MO, USA) supplemented with heat-inactivated fetal bovine serum (FBS; Moregate Exports, Qld, Australia) in a humidified atmosphere at 37°C and 5% CO_2.

Characterisation of KOPM88 cells

Morphological and cytochemical studies. Cytospin preparation, Giemsa staining, cytochemical staining for MPO and light microscopic examination were done using standard methods. Ultrastructural analysis was performed as follows. KOPM-88 cells were fixed in 2·5% glutaraldehyde in 0·1-mol/l sodium cacodylate buffer (pH 7·2), for 1 h. After washing, the cells were postfixed in 1% osmium tetroxide for 2 h, stained en bloc with uranyl acetate, dehydrated in a series of graded ethanol solutions and embedded in an Epon/Araldite mixture. Ultrathin sections were stained with lead citrate and examined under an electron microscope (Nippon Denshi EX-200, Tokyo, Japan).

Cell proliferation assay. A total of 5×10^3 KOPM88 cells were incubated with 100 μl of RPMI 1640 medium containing 10% FBS with or without the following cytokines (noted below) in flat bottomed 96-well tissue culture plates (Corning Inc., Corning, NY, USA), with 16 wells used for each group. On day 0 and day 5, MTT (3-(4,5-dimethylthyazol-2-yl)-5-(3-carboxymethoxyphenyl)-tetrazolium) assays were performed (Cell Titer 96 Aqueous One Solution Cell Proliferation Kit; Promega Corp., Madison, WI, USA) and measured at O.D.490. The cytokines and their concentration were as follows: human tumour necrosis factor-α (TNFα; Diaclone Research, Cedex, France) 10 ng/ml, human granulocyte colony-stimulating factor (G-CSF; Chugai Pharmaceutical Co., Ltd, Tokyo, Japan) 100 ng/ml, human granulo-macrophage colony-stimulating factor (GM-CSF; Diaclone Research) 10 ng/ml. Growth rates were calculated, and results were expressed as the mean ± standard deviation (SD) of five replicates. Statistical significance ($P < 0·001$) was determined using the Dunnett multiple comparison test of means.

Karyotyping. KOPM-88 cells were processed using a direct method and banded using the trypsin-Giemsa method. The karyotypes were described according to the International System for Cytogenetic Nomenclature (Shaffer & Tommerup, 2005).

Flow cytometry. For cell surface antigens (CD13, CD33), 1×10^6 cells were washed and suspended in RPMI medium containing 10% FBS and 0·1% sodium azide. After 30 min of incubation with the primary antibodies (noted below) and washing, fluorescein-isothiocyanate (FITC)-conjugated secondary antibodies were added and incubated for 30 min. For intracellular antigens [myeloperoxydase (MPO), myeloid/histiocyte Antigen (MHA), neutrophil elastase (NE)], 1×10^6 cells were fixed and permeabilised using a commercial kit (DAKO Intrastain; DakoCytomation, Glostrup, Denmark) according to the manufacturer's recommendations. For MPO, a monoclonal antibody (MoAb) against MPO directly conjugated with FITC was used. For MHA and NE, the samples were incubated for 30 min with the primary antibodies (noted below) and washed, then the FITC-conjugated secondary antibodies were added and the samples were incubated for 30 min. The samples were evaluated using a COULTER EPICS XL-MCL Flow Cytometer (Beckman Coulter, Inc., Fullerton, CA, USA) and SYSTEM II Software (Beckman Coulter, Inc.).The following antibodies were used: anti-MHA/clone MAC387 (Dako Cytomation), FITC-conjugated polyclonal rabbit anti-mouse immunoglobulins/F-0313 (Dako Cytomation), FITC-conjugated monoclonal mouse anti-human MPO/clone MPO-7 (Dako Cytomation), and FITC-conjugated negative control antibody mouse IgG1 (Dako Cytomation)

Cytogenetic analysis of MLL *gene*

Southern blotting. Genomic DNA was extracted from KOPM-88 cells and two control cell lines (positive control: KOCL-69, negative control: KOPT-K1) using standard procedures. A total of 15 μg of genomic DNA was digested to completion with BamHI. The enzyme digests were separated using electrophoresis on 0·7% agarose gels and blotted onto nylon membrane (GE Healthcare Bio-Sciences Corp, Piscataway, NJ, USA), then hybridised to probes. A 0·9-kb *MLL* cDNA probe (Yamamoto *et al*, 1993, 1994) was used for the hybridisation. Southern blotting, probe radiolabelling, hybridisation, and autoradiography were performed using standard techniques.

Fluorescence in situ hybridisation (FISH). Cell preparation and dual-colour FISH were performed as previously described (Stasi *et al*, 1997). To detect rearrangements in the *MLL* gene, two probes were selected: S1363, a cosmid mapping to the NotI–NotI region of exon 1 of the *MLL* gene, and LB140, a cosmid mapping to the NotI–NotI region 6·5 kb telomeric to the 3′ terminal of *MLL* gene. S1363 was labelled with biotin-16-dUTP, and LB140 was labelled with digoxigenin-11-dUTP using nick

translation. Hybridisation signals were visualised using immunofluorescence with neutravidin-FITC and rhodamine-conjugated anti-digoxygenin antibodies. The nuclei and chromosomes were counterstained using DAPI (4,6-diaminido-2-phenylindole). The slides were viewed using a fluorescence microscope equipped with a triple-band pass filter for the simultaneous excitation of FITC, rhodamine and DAPI.

Reverse transcription (RT) and nested polymerase chain reaction (PCR). Total RNA was isolated using a commercial kit (ISOGEN; Nippongene Co., Ltd., Tokyo, Japan) and reverse transcription was performed using a commercial kit (cDNA synthesis kit; GE Healthcare Bio-Sciences KK, Piscataway, NJ, USA) at 37°C for 1 h to obtain the cDNA. The cDNA was amplified by nested PCR using *Taq* DNA polymerase (Toyobo, Osaka, Japan). The PCR primer set for the first round of amplification was 3·1c (5′-AGGAGAGAGTTTACCTGCTC-3′) from exon 3 and 5·3 (5′-GGAAGTCAAGCAAGCAGGTC-3′) from exon 5; the primer set for the second round of amplification was 6·1 (5′-GTCCAGAGCAGAGCAAACAG-3′) from exon 6 and 3·2c (5′-ACAGATGGATCTGAGAGG-3′) from exon 3 (Schichman *et al*, 1994). PCR was performed for 35 cycles (95°C, 1 min; 53°C, 1 min; 72°C, 1 min) for the first round and 30 cycles (95°C, 1 min; 60°C, 1 min; 72°C, 1 min) for the second round. The PCR products were analysed using 2% agarose gel electrophoresis.

Sequence analysis. The presence of PTD was confirmed by direct sequencing of the PCR products. The PCR products were purified, then sequenced using the MegaBACE 1000 DNA sequencing system (GE Healthcare Bio-Sciences KK).

Transplantation of KOPM88 cells into immunosuppressed mice

Mice. Male NOD/SCID mice (gifted by Dr Nobumichi Hozumi, Tokyo Science University, Chiba, Japan) were maintained under specific pathogen-free conditions.

Transplantation of KOPM-88 cells. KOPM-88 cells were incubated with RPMI 1640 tissue culture medium (10% FBS), with or without the cytokines noted below, for 5 d. A total of 5×10^7 KOPM-88 cells were suspended in 100 μl of RPMI 1640 tissue culture medium. 8- to 10-week-old NOD/SCID mice were injected either intraperitoneally (i.p.) or intravenously via the dorsal tail vein (i.v.) with KOPM-88 cells. When the condition of the mice deteriorated, the mice were killed and necropsied after blood sampling by ventricular puncture. The control mice were injected with RPMI 1640 medium only. The cytokines and their concentration were as follows: human TNFα 10 ng/ml; human G-CSF, 100 ng/ml; human GM-CSF, 10 ng/ml.

In vivo *cytokine treatment of tumour bearing mice.* A total of 5×10^6 KOPM-88 cells were prepared and transplanted via the dorsal tail vein as described above. Beginning 4 weeks after transplantation, the mice were subcutaneously treated with human TNFα (500 ng/head/dose) and human G-CSF (10 μg/head/dose) once a week. The control mice only received phosphate-buffered saline.

Histopathology. The cytospin slides were stained with Giemsa stain. Histological sections of organs and tumours from NOD/SCID mice were prepared and stained with haematoxylin and eosin (HE) using standard methods. Immunohistochemistry was performed using the following antibodies: anti-human CD45RB monoclonal antibody (Dako Cytomation), anti-human MPO monoclonal antibody (Dako Cytomation), anti-human CD4 monoclonal antibody (Nichirei Bioscience Inc., Tokyo, Japan), anti-human CD15 monoclonal antibody (Becton Dickinison Immunocytometry Systems, San Jose, CA, USA), anti-human CD68 monoclonal antibody (Dako Cytomation) and horseradish peroxidase-conjugated secondary antibody (Dako Cytomation). Diaminobenzidine (3,3 DAB 4HCL; Wako, Tokyo, Japan) and H_2O_2 were used for colour development.

Results

Establishment and characteristics of KOPM-88 cell line

After 4 months of primary culture, the leukaemic cells derived from the relapsed patient with AML entered a constant proliferating state in RPMI 1640 medium supplemented with 10% FBS and the cells were passaged every 4–5 d at a 1:6 dilution. This resulted in the establishment of a permanent AML cell line, subsequently referred to as KOPM-88. Although the KOPM-88 cells were derived from a bulk cultivation (not a single-cell cloning), the immunophenotypes and ultrastractural morphology of the KOPM-88 cells had not changed significantly after the twenty-fourth passage. For optimum proliferation, the culture medium was exchanged every 4–5 d and the cell density was adjusted to $0{\cdot}5–1{\cdot}5 \times 10^6$ cells/ml. The cells could be frozen in FBS with 10% (v/v) dimethyl sulphoxide and stored over liquid nitrogen, then successfully recovered. Although KOPM-88 cells could be propagated without any exogenous cytokines, some cytokines affected cell proliferation (Fig 1). G-CSF and GM-CSF significantly accelerated proliferation while TNFα significantly suppressed the growth of KOPM-88 cells.

The effects of cytokines on myeloid specific antigens and enzymes, measured by flow cytometry, are shown in Fig 2. Five days of treatment with TNFα slightly increased the expression of MPO, NE and MHA (data not shown), and the effects were enhanced by G-CSF and GM-CSF. On the other hand, treatment with G-CSF alone, GM-CSF alone, or a combination of G-CSF and GM-CSF did not affect the expression of MPO, NE, or MHA (data not shown). Under standard culture conditions, KOPM-88 cells have a round-to-oval cell shape and exist as single cells that often form aggregates. Giemsa

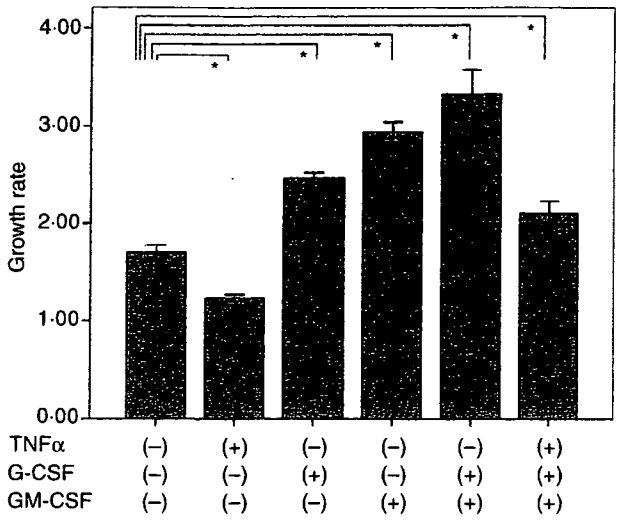

Fig 1. Proliferative responses of KOPM-88 cells to haematopoietic cytokines.KOPM-88 cells were cultured with the cytokines alone or in combination. See the Materials and methods section for details and cytokine concentrations. The growth rate at 5 d was measured using an MTT assay. Each bar represents the mean value ± SD of the growth rate in five replicates. The comparisons with the control that are marked by asterisks were statistically significant according to Dunnett multiple comparison test of means, with $P < 0{\cdot}001$.

staining of KOPM-88 cells showed an eccentric oval-shaped large nucleus and rich basophilic cytoplasm with abundant granules, similar to the patient's leukaemic cells (Fig 3A). A cross section of KOPM-88 cells taken with an electron microscope is presented in Fig 3B. The most prominent feature of the KOPM-88 cells was the primary granules in the cytoplasm, although this feature was even more prominent in the leukaemic cells of the patient. Because of poor morphology, karyotyping was done in only 13 cells. A representative karyotype of the KOPM-88 cells was interpreted as 91,YY, t(X;11)(q24;q23), t(X;11)(q24;q23), +1p−, +1p−, −9, −9, +15, −20, and a translocation between chromosome 11 and chromosome X was assumed (data not shown). However, further analysis of *MLL* gene revealed a PTD of chromosome11 (discussed below). Epstein–Barr virus (EBV) infection was excluded by immunohistochemistry against EBV nuclear antigen 2 (EBNA2) and latent-membrane protein-1 (LMP-1) and the *in situ* hybridisation of EBV-encoded RNA (EBER) (data not shown). The immunophenotypes of the KOPM-88 cells and the leukaemia cells from the patient are presented in Table I. In addition to being positive for myeloid antigens like CD13 and CD33, the KOPM-88 cells were also positive for CD4 and CD25.

MLL gene rearrangement in KOPM-88 cell line

Figure 4 shows the results of a Southern blot analysis of KOPM-88 cells and two control cell lines using the *MLL* cDNA probe on BamHI restriction enzyme digests. While a single 8·5-kb germ line band was detected in the negative control cell line KOPT-K1 (lane 3), two rearrangement bands in addition to the germ-line band were detected in KOPM-88 cells (lane 1), as well as in the positive control cell line KOCL-69 (lane 2). KOPT-K1 (Dong *et al*, 1995) is a cell line derived from a T cell ALL patient, which is known to have t(11;14)(p13;q11) but no *MLL* gene rearrangement. KOCL-69 (Yamamoto *et al*, 1994) is a cell line carrying t(4;11)(q21;q23) with confirmed *MLL* gene rearrangement,

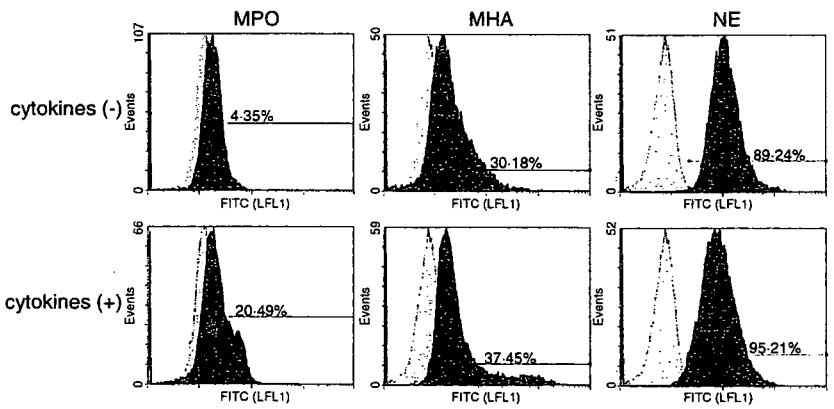

Fig 2. Effects of various cytokines on KOPM-88 cell surface antigen expression, as determined using flow cytometry. MPO, myeloperoxydase, MHA, myeloid/histiocyte antigen, NE, neutrophil elastase. KOPM-88 cells after 5 d of culture with or without cytokines were incubated with monoclonal antibodies (MoAbs) for the indicated antigens. A direct method was applied to detect MPO and an indirect method was applied to detect MHA and NE. Cytokine (+) indicates a combination of TNFα, G-CSF, and GM-CSF (see the Materials and methods section for the cytokine concentrations). For MPO, the dark grey area indicates a direct FITC-conjugated MoAb for MPO, and the pale gray area indicates irrelevant mouse IgG1 that was used as a negative control. For MHA and NE, the dark grey area indicates incubation with a secondary antibody (anti-mouse IgG, FITC-conjugated) after incubation with MoAbs for the indicated antigens, and the pale gray area indicates incubation with only the secondary antibody. The percentages of antigen expressing cells are shown. The percentages of cells expressing these three antigens increased after 5 d of cytokine treatment.

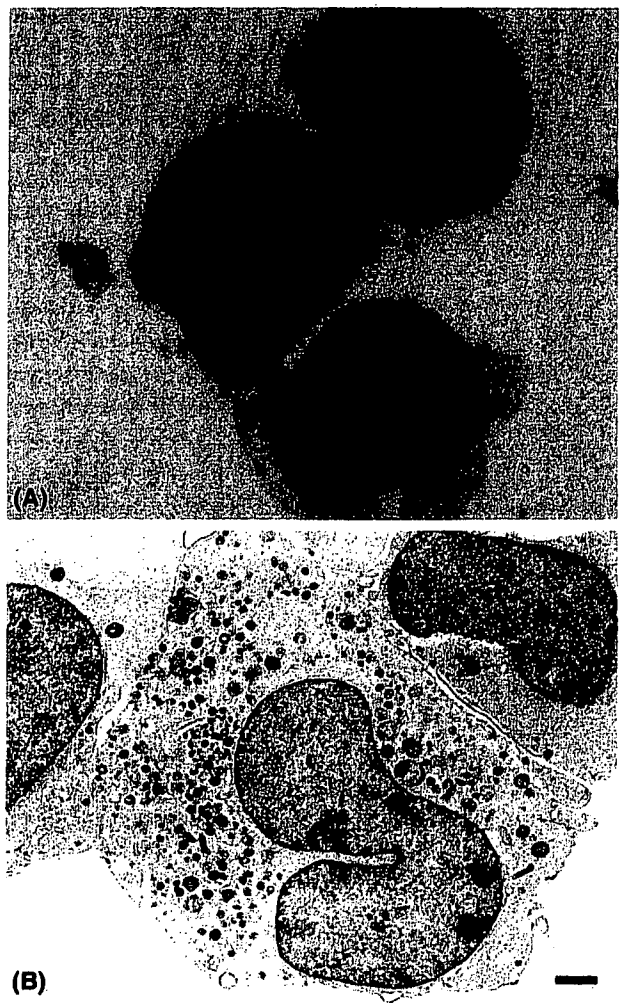

Fig 3. Morphology of KOPM-88 cells. (A) Light microscopy image of KOPM-88 cells (Giemsa stain of a cytospin preparation, original magnification: ×100). KOPM-88 cells are characterised by eccentric, oval shaped large nuclei and rich basophilic cytoplasm with abundant granules but without Auer bodies. (B) Electron microscopy image of KOPM-88 cells (magnification: ×4000). The black bar = 1 μm. A representative KOPM-88 cell exhibits an irregular nucleus with a nucleolus. Chromatin was slightly aggregated only at the submembrane region. Primary granules and rough endoplasmic reticulum are remarkable in the cytoplasm, but no Auer bodies are visible.

established from an ALL patient. FISH analysis of the KOPM-88 cells at interphase using two cosmid probes S1363 (green) and LB140 (red) is shown in Fig 5. The sites of the two probes were so close that the two signals overlapped in normal chromosome 11. In KOPM-88, the two signals were divided, indicating a partial duplication or insertion of the *MLL* gene. Two amplified products (approximately 250 and 450 bp) were obtained by nested PCR of KOPM-88 cDNA (Fig 6A). The DNA sequencing of the PCR products confirmed two patterns of PTD of the *MLL* gene, spanning exon 2 to exon 6 (exon 3 to exon 9 by new nomenclature), and exon 2 to exon 8 (exon 3 to exon 11 by new nomenclature) (Fig 6B).

Table I. Immunophenotypic characterisation of leukaemia cells and KOPM-88. The percentage of positive cells analysed by flow cytometry are shown. NT, not tested. Leukaemic cells at onset were positive for both myeloid antigen (CD33) and lymphoid antigens (CD2, 3, 4, 5). KOPM-88 cells were positive for myeloid antigens (CD11b, CD13) but only CD4 remained positive among the lymphoid antigens.

	% positive cells		
	Leukaemic cells		
	Onset	Relapse	KOPM-88
CD1	<10	<10	<10
CD2	31	<10	<10
CD3	29	<10	<10
CD4	65	35	91
CD5	15	<10	<10
CD7	<10	<10	<10
CD8	13	<10	<10
CD25	<10	<10	44
CD10	<10	<10	<10
CD19	<10	<10	<10
CD20	<10<	<10	<10
CD22	<10	<10	<10
CD11b	<10	<10	32
CD13	67	75	97
CD14	<10	<10	<10
CD33	<10	45	98
CD34	NT	<10	<10
CD36	<10	<10	<10
CD41	<10	<10	<10
HLA-DR	<10	<10	<10

Transplantation of KOPM88 cells to immunodeficient mice

All of the 15 mice that received KOPM-88 cells intraperitoneally (i.p. group) deteriorated 60–70 d after transplantation. Marked accumulations of bloody ascites were observed, and autopsies revealed intraperitoneal tumour masses with retroperitoneal invasion (Fig 7A and B), and systemic lymph node swelling. One mouse also had a tumour mass inside its spleen. Of the 27 mice (89%) that received KOPM-88 cells intravenously (i.v. group), 24 suffered paralysis of the hind limbs 60–80 d after transplantation. Autopsies and histological evaluations revealed that the paralysis was caused by tumour invasion from the bone marrow into the epidermal space around the spinal cord (Fig 8A). The mice were not irradiated because irradiation (γ ray, 1·13 Gy) before the innoculation of KOMP-88 cells did not affect the engraftment efficiency or the number of days before paralysis (data not shown). In both the i.p. and i.v. groups, histological preparations showed human CD45RB positive tumour cells in tumour mass, lymph nodes, spleen and bone marrow (Fig 8B and C). KOPM-88-like tumour cells were also found in cytospin preparations of peripheral blood monocytes. These results suggest that the transplanted KOPM-88 cells caused a leukaemic state in NOD/SCID mice. Immunohistochemistry showed that some of the tumour cells

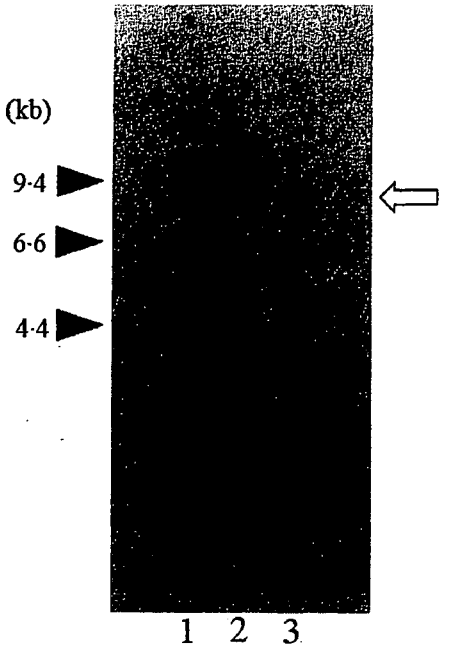

Fig 4. Southern blot analysis showing *MLL* gene rearrangement in KOPM-88 cells. A negative control cell line KOPT-K1 (lane3), shows only a germline band of 8·5-kb (white arrow). KOPM-88 cells (lane 1), and a positive control cell line KOCL-69 (lane 2), show two rearrangement bands (approximately 6 kb and 12 kb in lane 1 and approximately 5 kb and 12 kb in lane 2) in addition to the germ line band. KOPT-K1, used as a negative control, is a T cell ALL cell line without *MLL* gene rearrangement. KOCL-69, used as a positive control, is an ALL cell line carrying t(4;11)(q21;q23) with confirmed *MLL* rearrangement.

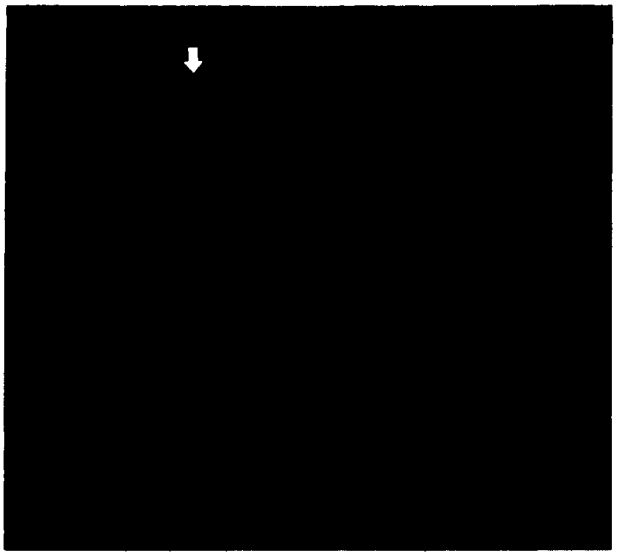

Fig 5. Dual colour FISH analysis of a KOPM-88 cell at interphase using two cosmid probes: S1363 (green) and LB140 (red). The sites of the two probes were so close that the two signals overlapped in normal chromosome 11. Note the divided signals (white arrow), indicating a duplication or insertion of the *MLL* gene.

were positive for MPO, CD4, CD15 and CD68 (Fig 9A and C). In order to investigate the effect of human cytokines in our animal model, we selected the combination of TNFα, G-CSF and GM-CSF because this combination showed a stronger effect on myeloid differentiation markers than any of each

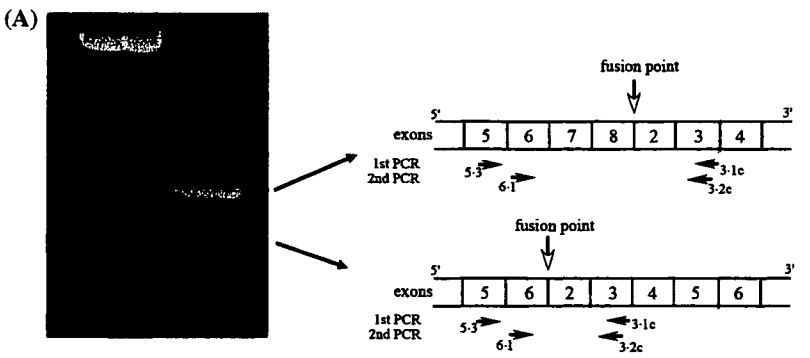

(B) (1)
Exon6 Exon2
AAA CCA AAA GAA AAG / GAT GAG CAA TTC TTA
(2)
Exon8 Exon2
AGT GGG CAT GTA GAG / GAT GAG CAA TTC TTA

Fig 6. Partial tandem duplication (PTD) of the *MLL* gene in KOPM-88 cells. (A) Nested PCR analysis of the *MLL* gene of KOPM-88 cDNA using the sets of primers noted in the Materials and Methods section. The result of the second PCR is shown in the photograph. Two amplified products (approximately 250 bp and 450 bp) were obtained. The schematic structure of the rearranged *MLL* mRNA predicted from each band is shown on the right side. The boxes with numbers represent the exons of the *MLL* gene. The white arrows indicate the fusion points and the black arrows indicate the sites of the primers used for the PCR. The primer name is shown below each arrow. The primer sequences are given in the Materials and methods section. (B) Two patterns for the *MLL*-PTD were confirmed using DNA sequence analysis of the nested PCR products. In-frame fusions of *MLL* exon 6 with exon 2 (1) and exon 8 with exon 2 (2) were detected.

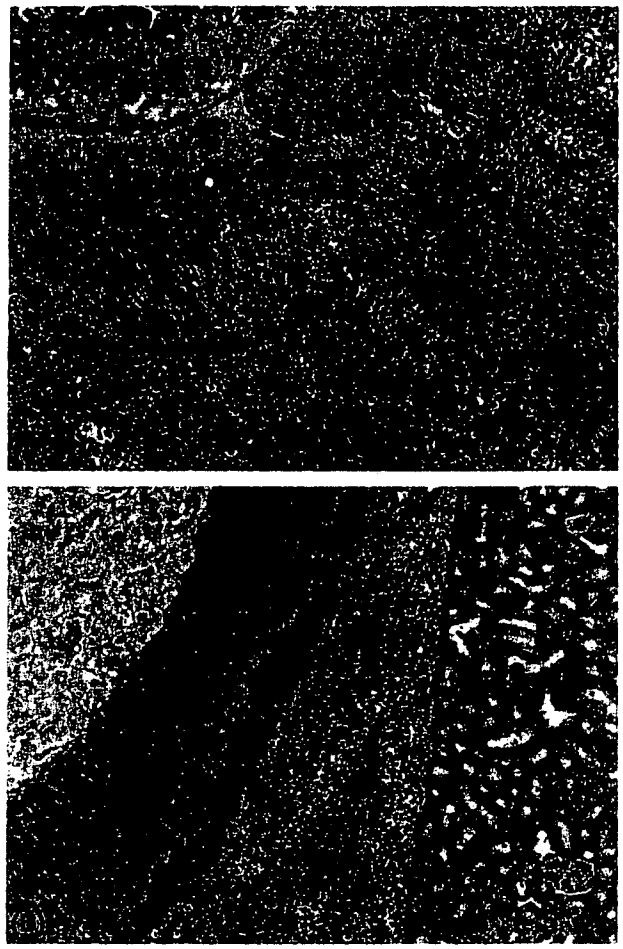

Fig 7. Representative histopathological appearances of the growth and invasion of KOPM-88 cells engrafted intraperitoneally in NOD/SCID mice. (A) KOPM-88 cells invading the muscular layer of the intestine (HE stain, original magnification: ×20). (B) Retroperitoneal invasion of KOPM-88 cells (HE stain, original magnification: ×20).

cytokine in the *in vitro* study using flow cytometry. Human cytokine treatment (TNFα, G-CSF and GM-CSF) of the KOPM-88 cells prior to transplantation did not affect the number of days required for the mice to deteriorate, or the histological features of the tumour. Nevertheless, immunohistochemistry revealed that CD15 and CD68 expression was significantly augmented on the tumour cells in the cytokine treatment group (Fig 9A–D).

Tumour cells from KOPM-88 bearing mice that received human cytokines (TNFα and G-CSF) *in vivo* also showed increased expressions of CD15 and CD68 than tumour cells from control mice (Fig 10A–D). Furthermore, the condition of the mice in the *in vivo* treatment group tended to deteriorate earlier than in the control group (data not shown).

Discussion

Alteration of the *MLL* gene at 11q23 is common among haematological malignancies, and its role in oncogenesis has been investigated. Among the many types of *MLL* gene alterations, PTD has recently been reported to have a mechanistically distinct contribution to leukaemogenesis (Whitman *et al*, 2005). From a clinical point of view, the prognostic impact of *MLL*-PTD in AML is still controversial (Shiah *et al*, 2002), but some study groups have reported that AML patients with *MLL*-PTDs exhibit shorter remission duration or shorter overall survival in an adult subgroup (Dohner *et al*, 2002). We established a novel cell line, KOPM-88, carrying an *MLL*-PTD that was derived from the peripheral blood of a paediatric AML patient. At the onset of the disease, the patient was diagnosed with acute promyelocytic leukaemia because of severe DIC and hypergranular cytoplasm of the leukaemic cells. However, the absence of an *RARA* gene abnormality and the failure of the patient to respond to all-*trans* retinoic acid (ATRA) treatment, led to a subsequent diagnosis of unclassified AML (Nakata *et al*, 1999). Considering the fact that only four cell lines with *MLL*-PTDs have been reported (Drexler *et al*, 2004), KOPM-88 is expected to serve as a useful tool for investigating the mechanisms of oncogenesis arising from *MLL*-PTDs.

KOPM-88 cells have both morphological and cytochemical myeloid characteristics. As for their immunophenotype, mixed lineage antigen expression has been reported in leukaemic cells with *MLL* gene involvement (Swansbury *et al*, 1998), but some studies in AML patients have reported no significant difference in lymphoid antigen expression in patients with or without *MLL* gene involvement (Baer *et al*, 1998; Munoz *et al*, 2003). In our study, although the leukaemic cells at onset expressed some lymphoid markers (CD2, CD3 and CD5) in addition to myeloid markers (CD13 and CD33), the leukaemic cells at relapse and the KOPM-88 cells expressed only myeloid markers. The KOPM-88 cells were positive for the T-lineage marker CD4, but CD4 was also positive in monocytic cells. The KOPM-88 cells also expressed other markers for monocytic differentiation, CD11b and CD25. Although the KOPM-88 cells were cytokine independent, their growth was accelerated by G-CSF and GM-CSF, indicating a myeloid character. Southern blot analysis confirmed the *MLL* gene rearrangement in the KOPM-88 cells and the leukaemic cells of the patient. FISH analysis and RT-PCR/DNA sequencing analysis revealed PTD of exon 2 to exon 6 (exon 3 to exon 9 by new nomenclature; Basecke *et al*, 2006), and exon 2 to exon 8 (exon 3 to exon 11 by new nomenclature) of the *MLL* gene. Two rearrangement bands of 4·4–6·6 kb and over 9·4 kb were observed by Southern blot analysis (Fig 4). These results were compatible with the structure of *MLL*-PTD of exon 2 to exon 6 and exon 2 to exon 8, where the 5′ portion of intron 6 was fused with 3′ portion of intron 1 not containing BamHI restriction site and 5′ portion of intron 8 was fused with 3′ portion of intron 1 containing BamHI restriction site (Zieminvan der Poel *et al*, 1991; Rasio *et al*, 1996). Obtaining two or more PTD cleavage patterns from one case or cell line is not uncommon because of alternate splicing (Yu *et al*, 1996). A long range PCR study to estimate any alternative splicing was not performed, but we consider this interpretation of the

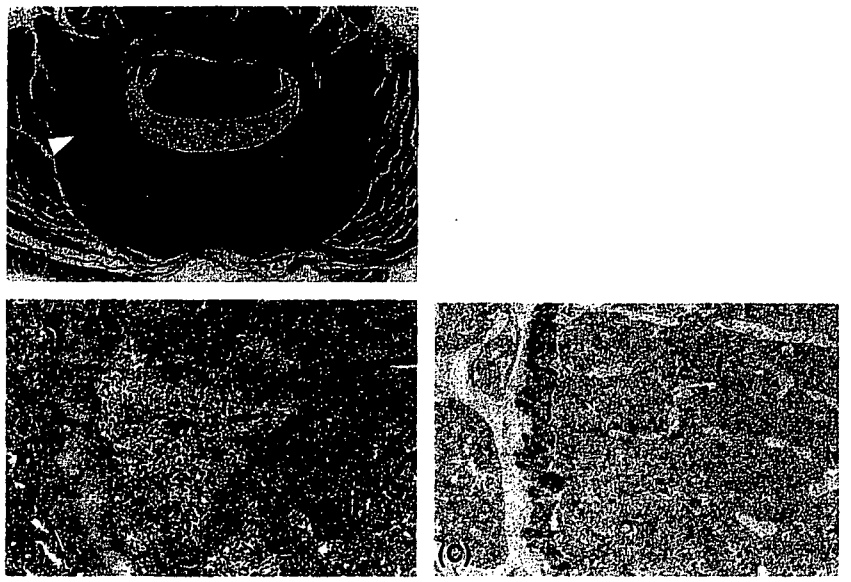

Fig 8. Representative histopathological appearances of the growth and invasion of KOPM-88 cells engrafted intravenously in NOD/SCID mice. (A) Invasion of KOPM-88 cells into the epidermal space of an NOD/SCID mouse with paralysis of the hind extremities (HE stain, original magnification: ×4). White arrowhead indicates invaded area. (B) Invasion of KOPM-88 cells in bone marrow. The bone marrow of the NOD/SCID mouse has been infiltrated by large, atypical blasts (HE stain, original magnification: ×20). (C) Immunohistochemistry with anti-human CD45RB antibody in the same sample shown in (B). The KOPM-88 cells are positive for human specific CD45RB (original magnification: ×20).

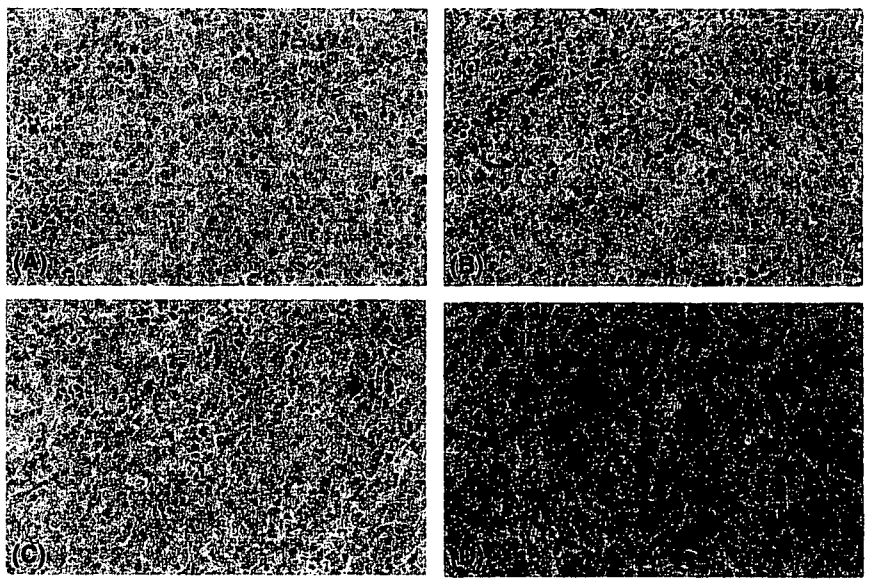

Fig 9. Effects of *in vitro* combined cytokine treatment on KOPM-88 cells engrafted in NOD/SCID mice. All tissues were excised from intraperitoneal tumours mass of IP group mice. The detailed method of immunohistochemistry and cytokine treatment is described in Materials and methods. Augmented expressions of both CD15 (A and B) and CD 68 (C and D) on the cytokine-treated cells (B and D) were detected compared with untreated cells (A and C) (original magnification: ×25).

RT-PCR results to be feasible because the FISH study showed only one allele, suggesting *MLL*-PTD.

Our initial observation of the KOPM-88 karyotype using the banding method was t(X;11)(q24;q23), but further *MLL* gene analysis revealed PTD of the *MLL* gene and a FISH study excluded the possibility of the co-existence of a translocation with the PTD. The poor morphology limited our initial interpretation of the karyotype. Former studies have revealed the importance of molecular studies, such as Southern blotting and FISH, in evaluating *MLL* rearrangements in haematological malignancies, as about 50% of *MLL* rearrangements revealed by molecular studies could not be detected using

Razzouk, B.I., Estey, E., Pounds, S., Lensing, S., Pierce, S., Brandt, M., Rubnitz, J.E., Ribeiro, R.C., Rytting, M., Pui, C.H., Kantarjian, H. & Jeha, S. (2006) Impact of age on outcome of pediatric acute myeloid leukemia: a report from 2 institutions. *Cancer*, **106**, 2495–2502.

Rubnitz, J.E., Raimondi, S.C., Tong, X., Srivastava, D.K., Razzouk, B.I., Shurtleff, S.A., Downing, J.R., Pui, C.H., Ribeiro, R.C. & Behm, F.G. (2002) Favorable impact of the t(9;11) in childhood acute myeloid leukemia. *Journal of Clinical Oncology*, **20**, 2302–2309.

Saito, H., Bourinbaiar, A., Ginsburg, M., Minato, K., Ceresi, E., Yamada, K., Machover, D., Breard, J. & Mathe, G. (1985) Establishment and characterization of a new human eosinophilic leukemia cell line. *Blood*, **66**, 1233–1240.

Schichman, S.A., Caligiuri, M.A., Gu, Y., Strout, M.P., Canaani, E., Bloomfield, C.D. & Croce, C.M. (1994) ALL-1 partial duplication in acute leukemia. *Proceedings of the National Academy of Sciences of the United States of America*, **91**, 6236–6239.

Schnittger, S., Wormann, B., Hiddemann, W. & Griesinger, F. (1998) Partial tandem duplications of the MLL gene are detectable in peripheral blood and bone marrow of nearly all healthy donors. *Blood*, **92**, 1728–1734.

Shaffer, L.G. & Tommerup, N. (ed.) (2005) *An International System for Human Cytogenetic Nomenclature*. S. Karger AG, Basel.

Shiah, H.S., Kuo, Y.Y., Tang, J.L., Huang, S.Y., Yao, M., Tsay, W., Chen, Y.C., Wang, C.H., Shen, M.C., Lin, D.T., Lin, K.H. & Tien, H.F. (2002) Clinical and biological implications of partial tandem duplication of the MLL gene in acute myeloid leukemia without chromosomal abnormalities at 11q23. *Leukemia*, **16**, 196–202.

Shih, L.Y., Liang, D.C., Fu, J.F., Wu, J.H., Wang, P.N., Lin, T.L., Dunn, P., Kuo, M.C., Tang, T.C., Lin, T.H. & Lai, C.L. (2006) Characterization of fusion partner genes in 114 patients with de novo acute myeloid leukemia and MLL rearrangement. *Leukemia*, **20**, 218–223.

Shultz, L.D., Schweitzer, P.A., Christianson, S.W., Gott, B., Schweitzer, I.B., Tennent, B., McKenna, S., Mobraaten, L., Rajan, T.V., Greiner, D.L. & Leiter, E.H. (1995) Multiple defects in innate and adaptive immunologic function in NOD/LtSz-scid mice. *Journal of Immunology*, **154**, 180–191.

Stasi, R., Bruno, A., Venditti, A., Del Poeta, G., Aronica, G., Cox, M.C., Maffei, L., Catalano, G., Zangrilli, D. & Amadori, S. (1997) A microgranular variant of acute promyelocytic leukemia with atypical morpho-cytochemical features and an early myeloid immunophenotype. *Leukemia Research*, **21**, 575–580.

Swansbury, G.J., Slater, R., Bain, B.J., Moorman, A.V. & Secker-Walker, L.M. (1998) Hematological malignancies with t(9;11)(p21–22;q23) – a laboratory and clinical study of 125 cases. European 11q23 Workshop participants. *Leukemia*, **12**, 792–800.

The Groupe Francais de Cytogenetique Hematologique (1996) Cytogenetic abnormalities in adult acute lymphoblastic leukemia: correlations with hematologic findings outcome. A Collaborative Study of the Group Francais de Cytogenetique Hematologique. *Blood*, **87**, 3135–3142.

Traweek, S.T., Arber, D.A., Rappaport, H. & Brynes, R.K. (1993) Extramedullary myeloid cell tumors. An immunohistochemical and morphologic study of 28 cases. *American Journal of Surgical Pathology*, **17**, 1011–1019.

Whitman, S.P., Liu, S., Vukosavljevic, T., Rush, L.J., Yu, L., Liu, C., Klisovic, M.I., Maharry, K., Guimond, M., Strout, M.P., Becknell, B., Dorrance, A., Klisovic, R.B., Plass, C., Bloomfield, C.D., Marcucci, G. & Caligiuri, M.A. (2005) The MLL partial tandem duplication: evidence for recessive gain-of-function in acute myeloid leukemia identifies a novel patient subgroup for molecular-targeted therapy. *Blood*, **106**, 345–352.

Yamamoto, K., Seto, M., Komatsu, H., Iida, S., Akao, Y., Kojima, S., Kodera, Y., Nakazawa, S., Ariyoshi, Y., Takahashi, T. & Ueda, R. (1993) Two distinct portions of LTG19/ENL at 19p13 are involved in t(11;19) leukemia. *Oncogene*, **8**, 2617–2625.

Yamamoto, K., Seto, M., Iida, S., Komatsu, H., Kamada, N., Kojima, S., Kodera, Y., Nakazawa, S., Saito, H., Takahashi, T. & Ueda, R. (1994) A reverse transcriptase-polymerase chain reaction detects heterogeneous chimeric mRNAs in leukemias with 11q23 abnormalities. *Blood*, **83**, 2912–2921.

Yu, M., Honoki, K., Andersen, J., Paietta, E., Nam, D.K. & Yunis, J.J. (1996) MLL tandem duplication and multiple splicing in adult acute myeloid leukemia with normal karyotype. *Leukemia*, **10**, 774–780.

Ziemin-van der Poel, S., McCabe, N.R., Gill, H.J., Espinosa, III R., Patel, Y., Harden, A., Rubinelli, P., Smith, S.D., LeBeau, M.M., Rowley, J.D. & Diaz, M.O. (1991) Identification of a gene, MLL, that spans the breakpoint in 11q23 translocations associated with human leukemias. *Proceedings of the National Academy of Sciences of the United States of America*, **88**, 10735–10739.